An Adaptive Threshold in Mammalian Neocortical Evolution

Eric Lewitus[1∞], Iva Kelava[1∞], Alex T. Kalinka[2], Pavel Tomancak[1], and Wieland B Huttner[1*]

[1]Max Planck Institute of Molecular Cell Biology and Genetics, Pfotenhauerstr. 108, 01307 Dresden, Germany

[2]Institut für Populationsgenetik, Vetmeduni Vienna, Veterinärplatz 1, 1210 Wien, Austria

[∞]These authors contributed equally

[*]Corresponding author

Abstract

Expansion of the neocortex is a hallmark of human evolution. However, it remains an open question what adaptive mechanisms facilitated its expansion. Here we show, using gyrencephaly index (GI) and other physiological and life-history data for 102 mammalian species, that gyrencephaly is an ancestral mammalian trait. We provide evidence that the evolution of a highly folded neocortex, as observed in humans, requires the traversal of a threshold of $\sim 10^9$ neurons, and that species above and below the threshold exhibit a bimodal distribution of physiological and life-history traits, establishing two phenotypic groups. We identify, using discrete mathematical models, proliferative divisions of progenitors in the basal compartment of the developing neocortex as evolutionarily necessary and sufficient for generating a fourteen-fold increase in daily prenatal neuron production and thus traversal of the neuronal threshold. Finally, using RNA-seq data from fetal human neocortical germinal zones, we show a genomic correlate to the neuron threshold in the differential conservation of long intergenic non-coding RNA.

(see arXiv:1304.5412)

Introduction

Development of the human neocortex involves a lineage of neural stem and progenitor cells that forms a proliferative region along the ventricular epithelium. The proliferation of cells within this region expands the neocortex by increasing neuron number. At the onset of mammalian cortical neurogenesis, neuroepithelial cells transform into radially oriented apical radial glia (aRG), which proliferate extensively at the apical surface of the ventricular zone and divide asymmetrically to self-renew and generate a neuron, intermediate progenitor (IP), or basal radial glia (bRG) (Franco and Müller, 2013). IP cells delaminate from the apical surface and translocate their nucleus to the basal region of the ventricular zone (VZ) to form a second germinal layer, the subventricular zone (SVZ), where they divide symmetrically to generate two neurons (Noctor et al., 2001; Miyata et al., 2004; Haubensak et al., 2004). Similarly to aRG cells at the ventricular surface, bRG cells divide asymmetrically, albeit abventricularly (Fietz et al., 2010; Hansen et al., 2010; Shitamukai et al., 2011; Wang et al., 2011); but contrary to aRG cells, bRG in the human may both divide symmetrically and generate neurons via transit-amplifying progenitors (TAPs), a cell-type that is not observed to originate basally in the mouse (Hansen et al., 2010). Furthermore, bRG, which maintain a single fiber ascending only to the basal surface in the mouse, may also be non-polar or bipolar in the macaque (Betizeau et al., 2013). The abventricular expansion of progenitors during cortical neurogenesis in humans further compartmentalizes the basal region into an inner (ISVZ) and outer SVZ (OSVZ), driving the radial fibers to have divergent, rather than parallel, trajectories to the cortical plate, and thus creating the folded cortical pattern observed in gyrencephalic species through the tangential expansion of migrating neurons (Smart et al., 2002; Borrell and Reillo, 2012; Lewitus et al., 2013). For this reason, and based on supporting evidence obtained in the gyrencephalic human and ferret and lissencephalic mouse, it was originally thought that an abundance of asymmetrically dividing bRG cells in the outer SVZ was an evolutionary determinant for establishing a relatively large and gyrencephalic neocortex (Fietz et al., 2010; Hansen et al., 2010; Reillo et al., 2011). But recent work in the lissencephalic marmoset (*Callithrix jacchus*) has shown that bRG cells may, in fact, exist in comparable abundance in both gyrencephalic and lissencephalic species (García-Moreno et al., 2012; Kelava et al., 2012) and so cannot alone be sufficient for either establishing or increasing cortical gyrification. Thus, despite considerable progress in the study of brain size evolution (Finlay and Darlington, 1995; Krubitzer and Kaas, 2005; Hager et al., 2012), the adaptive mechanism that has evolved along certain mammalian lineages to produce

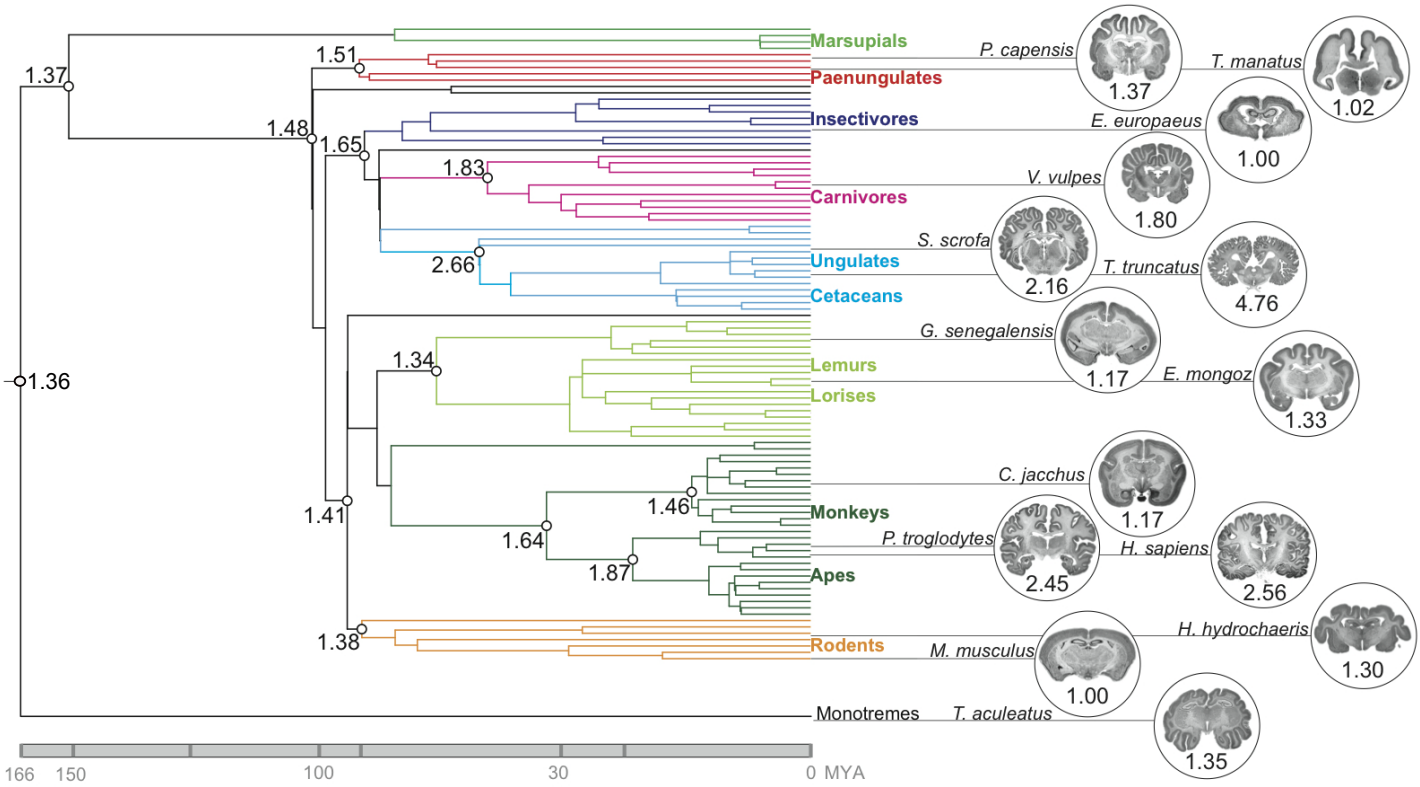

Figure 1: Ancestral reconstruction of GI values for 102 mammalian species. GI values were determined as illustrated in Figure S1 for the species listed in Table S1. Reconstructed GI values for putative ancestors are presented at selected internal nodes of the phylogenetic tree. MYA, million years ago; colors indicate taxonomic groups. Images of Nissl-stained coronal sections of representative species for each taxonomic group, downloaded from http://brainmuseum.org, along with respective GI values, are shown on the right.

a large and folded neocortex is not known.

In this study, we analyzed physiological and life-history data from 102 mammalian species (Table S1; Table S2; External Database 1). We show that a gyrencephalic neocortex is ancestral to all mammals (Figure 1) and that GI (Figure S1), like brain size, has increased and decreased along many mammalian lineages. These changes may be reliably characterized by convergent adaptations into two distinct physiological and life-history programs (Figure 2a), resulting in a bimodal distribution of mammalian species (Figure 2b) with a robust threshold value for both GI and neuron number (Figure 3). Traversal of the threshold requires greater neuron production per gestation day (Figure 4a,b), which we argue is necessitated by the evolution of increased proliferative potential in SVZ progenitors during cortical neurogenesis (Figure 5). Using fetal human transcriptome data from neocortical germinal zones, we show that long intergenic non-coding RNA (lincRNA) expressed during human neurogenesis are selectively lost in species below the neuron threshold. This provides evidence for the involvement of lincRNA in not only regulating, but also defining the neurogenic program of mammalian species.

The mammalian ancestor was gyrencephalic

We tested multiple evolutionary models for GI evolution. The model that conferred most power to explain GI values across the phylogeny while making the fewest assumptions about the data (i.e., had the lowest Akaike Information Criterion (AIC)) showed a disproportionate amount of evolutionary change to have occurred recently, rather than ancestrally, in mammals (Figure S2) and diverged significantly from a null model of stochastic evolution (Pagel, 1999). We identified a folded neocortex (GI =1.36 $\pm$ 0.16 s.e.m.) as an ancestral mammalian trait (Figure 1). It is apparent from ancestral and other internal node reconstructions (Figure S3) that GI is very variable, but also that reductions in the rate at which GI evolves have favored branches leading to decreases in GI (e.g., strepsirrhines and insectivores) and accelerations in that rate have favored branches leading to increases in GI (e.g., carnivores and caviomorphs). A simulation of the average number of total evolutionary transitions between GI values evidences more affinity for transitioning from high-to-low than low-to-high GI values: the majority of high-to-low transitions (58.3%) occurred in species with a GI $<$ 1.47; and the fewest transitions (16.7%) occurred across a threshold value of 1.5 (Figure S4). This indicates that, although there is an evident trend in mammalian history to become increasingly gyrencephalic, the most variability in GI evolution has been concentrated among species below a certain threshold value (GI = 1.5). We therefore present a picture of early mammalian history, contrary to those previously painted, but which is gathering evidence through novel approaches (O'Leary et al., 2013; Romiguier et al., 2013), that the Jurassic-era mammalian ancestor may, indeed, have been a large-brained species with a folded neocortex.

A threshold in cortical neuron number

The evolutionary effects of a folded neocortex on the behavior and biology of a species is not immediately clear. We therefore analyzed associations, across the phylogeny, of GI with discrete character states of 37 physiological and life-history traits (Table S2). Distinct sets of small but significant ($R^2 \leq 0.23$, $P < 0.03$) associations were found for species above and below a GI value of 1.5, indicating that these two groups of species adapt to their environments differently (Figure 2a). Both groups were sampled from across the phylogeny, showing no phylogenetic signal. Clustering analyses also supported a bimodal distribution above and below a threshold value of 1.5 (Figure 2b; Figure S5). To test the bimodal distribution explicitly, we regressed GI values against neuroanatomical traits and found that each scaling relationship could be explained comparably well by either a non-linear function (Figure 3a) or two grade-shifted linear functions, with the best-fit linear models drawing significantly different slopes (P

a

Trait	GI value			
	<1.31	1.31-1.47	1.64-2.94	>3
diurnality	P			
large litter size	P			
omnivory	P			
short maximum lifespan	P			
small body length	P			
small neonate brain weight	P			
leaves/branches/bark diet	P			
smallest body weight	P	P		
early age at eye opening	P	P		
early age at first breeding	P	P		
narrow habitat breadth	P	P		
nocturnality	P	P		N
short gestation length	P	P		
short juvenility	P	P		
short weaning period	P	P		
small brain weight	P	P		
small home range	P	P		
large population group size		P		
small litter size		P		
small social group size		P		
small weight at birth		P		
small weight at weaning		P		
vertebrate diet		P		
invertebrate diet		P		N
early female sexual maturity		P	P	
early male sexual maturity		P	P	
small interlitter interval		P	P	
fruit diet			P	
large home range			P	
medium body weight			P	
medium neonate brain weight			P	
moderate habitat breadth			P	
long maximum lifespan	N		P	P
large weight at birth	N		P	P
long juvenility		N	P	P
long weaning period			P	P
mixed activity timing			P	P
moderate age at first breeding			P	P
long gestation length			P	P
large social group size			P	P
large brain weight			P	P
medium interlitter interval				P
medium body length				P
late female sexual maturity				P
late male sexual maturity				P
wide habitat breadth				P
large body weight				P
large neonate brain weight				P

b

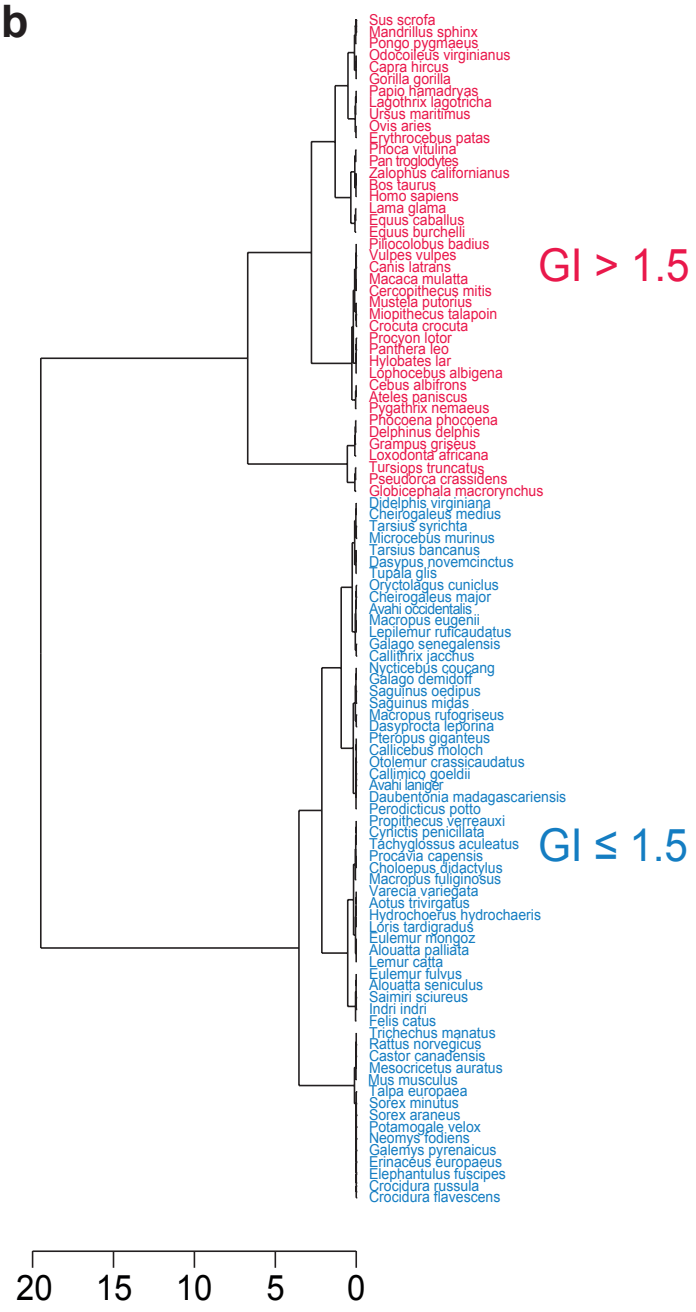

Figure 2: Clustering of GI values based on life-history association analysis (a) and minimum-energy distance (b). (a) Stochastic mapping of physiological and life-history traits with GI values for the 102 mammalian species listed in Table S1. GI values were separated into four groups based on clustering. Forty traits, each comprising 3 - 6 character states, were analyzed (see Table S2 for a complete list), and the states showing a significant positive (P, green) or negative (N, red) association with a group of GI values are shown. Note the major overlap between the two low-GI groups (10/27) and between the two high-GI groups (9/24), whereas only 3/48 character states are shared between GI groups ≤ 1.5 and > 1.5. (b) Hierarchical clustering based on minimum-energy distance of the GI values for 101 mammalian species. Note that the greatest clustering height is between species with GI values of ≤ 1.5 and > 1.5.

= 3.4 x 10^{-4}) for high-GI ($>$ 1.5) and low-GI ($<$ 1.5) species. (Figure 3b,c). By plotting GI as a function of cortical neuron number, we were able to demarcate, with two significantly different linear regressions for high- and low-GI species (T = 4.611, d.f. = 29, P = 2.8 x 10^{-4}), a cortical no-man's-land centered on an area approximating 1 $\pm$ 0.11 x 10^9 neurons and 1.56 $\pm$ 0.06 GI (Figure 3d). The deviation of these results from previous work, which have shown strong phylogenetic signals associated with both GI (Pillay and Manger, 2007; Zilles et al., 2013) and neuron counts (Azevedo et al., 2009), may be explained both by our more than 2-fold increase in sampled species and the *a priori* assumption of previous work that GI and neuron number evolve as a function of phylogeny. Variation in GI, therefore, has not evolved linearly across the phylogeny, but has in fact been differentially evolved in two phenotypic groups. Each group may be characterized not only by a high ($>$ 1.5) or low ($<$ 1.5) GI value, but also by a distinct constellation of other physiological and life-history traits which have accompanied each group over evolutionary time.

More efficient neurogenesis in large-brained species

By establishing an evolutionary threshold based on both degree of gyrencephaly and neuron number, we identified two neocortical phenotypic groups, which found support in their distinct life-history associations (see previous section). These groups could be further divorced by accounting for the amount of brain weight accumulated per gestation day - confident proxies for neonate brain weight and neurogenic period, respectively (Figure S6) - which we show to be, on average, 14-times greater in high- compared to low-GI species (Figure 4). Notably, each GI group is constituted by both altricial and precocial species, so the degree of pre- *versus* post-natal development is not enough to explain the discrepancy in brain weight per gestation day in each group. Rather, to explain the discrepancy, we introduced a deterministic model of cortical neurogenesis, using series summarizing seven neurogenic lineages and based on cell-cycle length, neuroepithelial founder pool size, neurogenic period, and estimates of relative progenitor-type population sizes (Table 1). We arrived at two models, based on the analysis of 16 species, that show the highest reliability for predicting cortical neuron numbers in a range of species: a mouse neurogenic program, which implicates only aRG, IP, and asymmetrically dividing bRG; and a human neurogenic program, which additionally implicates proliferating progenitors in the SVZ. Each model is defined by the proportional occurrence of each lineage in that model (Table 2). Using the mouse neurogenic program we were able to predict neuron counts within 2% of the observed counts for mouse and rat, but underestimated neuron counts by more than 80% in high-GI species (Figure 5; Table S3). Similarly, the human neurogenic program predicted neuron counts within 5% for all high-GI species, but overestimated neuron

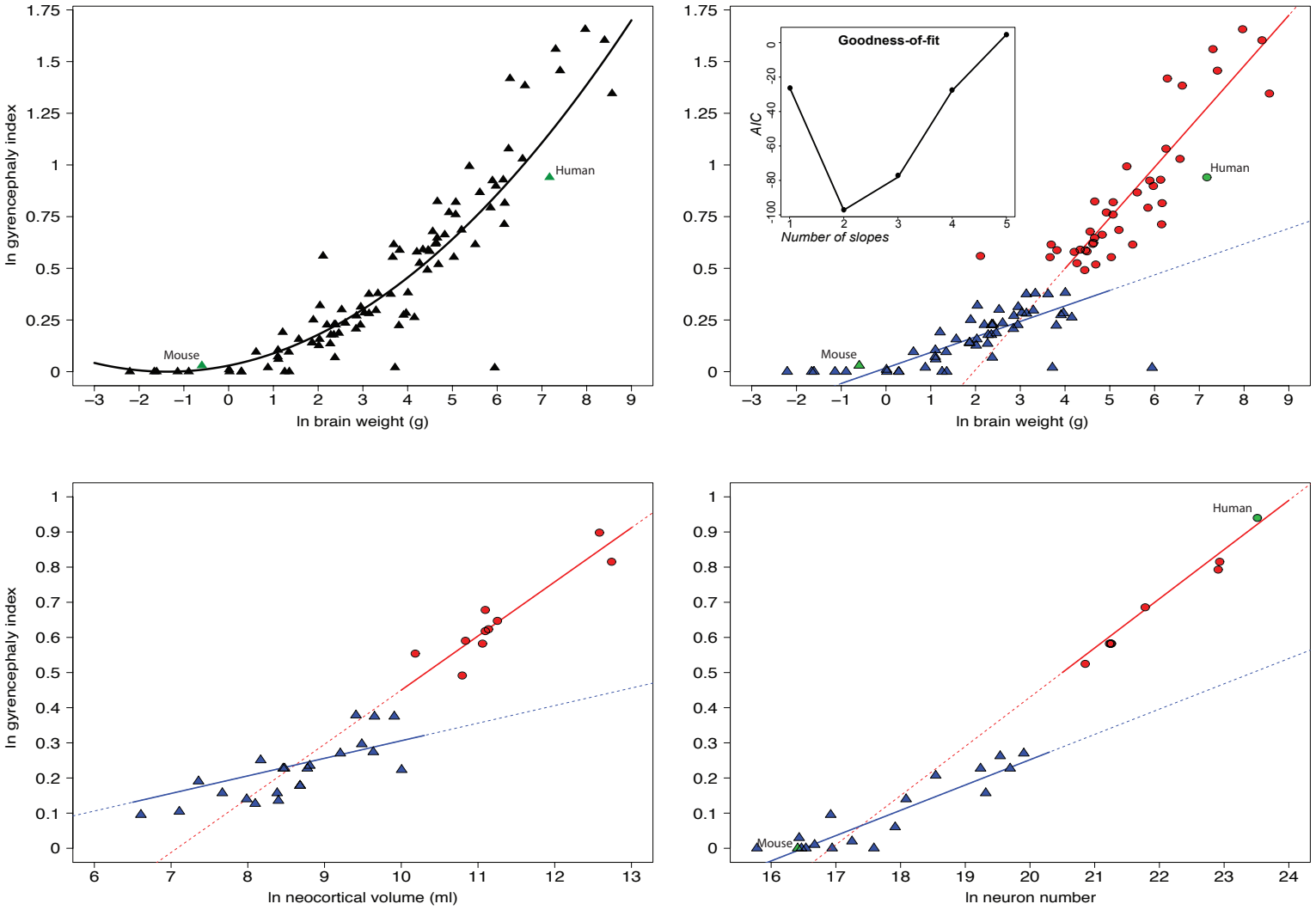

Figure 3: Ln-transformed plots showing GI values as a function of brain weight (a, b, 101 species), neocortical volume (c, 29 species) and cortical neuron number (d, 22 species). (a) Regression analysis using one non-linear fit for all values ($y = 0.018x^2 + 0.037x + 0.014$, $R^2 = 0.612$, $P = 6 \times 10^{-5}$); (b-d) regression analyses using two different linear functions (b, blue line: $y = 0.075x - 0.481$, $R^2 = 0.56$, $P = 4 \times 10^{-5}$, red line: $y = 0.245x + 0.018$, $R^2 = 0.73$, $P = 1 \times 10^{-5}$; c, blue line: $y = 0.050x - 0.194$, $R^2 = 0.21$, $P = 0.017$, red line: $y = 0.154x - 1.09$, $R^2 = 0.82$, $P = 0.004$; d, blue line: $y = 0.072x - 1.188$, $R^2 = 0.81$, $P = 1 \times 10^{-4}$; red line: $y = 0.140x - 2.370$, $R^2 = 0.98$, $P = 3 \times 10^{-5}$) for species with GI values of < 1.5 (blue triangles) and > 1.5 (red circles), respectively; mouse and human are indicated by green symbols. The inset in (b) shows the AIC values for models fitted with $1 - 5$ linear slopes; note that a two-slope model best explains the data. See Table S1 for data.

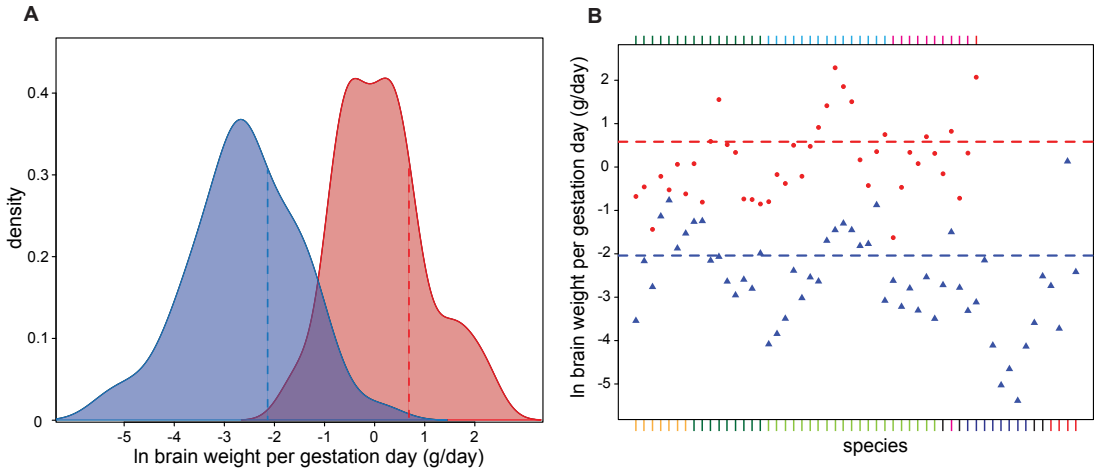

Figure 4: Brain weight per gestation day is considerably greater for high- versus low-GI species. (a) Ln-transformed density plot of brain weight per gestation day for 96 eutherian species listed in Table S1 with GI values of ≤ 1.5 (blue) and > 1.5 (red). Note the significantly different means for the two groups (dashed blue and red lines, T $= 5.16$, d.f. $= 41$, P $= 4 \times 10^{-5}$).(b) Ln-transformed plot of brain weight per gestation day for 96 mammalian species (see a). Dashed blue line, mean value for GI ≤ 1.5 (-2.04 $\pm$ 0.047, s.d.); red dashed line, mean value for GI > 1.5 (0.583 $\pm$ 0.050, s.d.). The colors in the index refer to species in Figure 1. See Table S1 for data.

counts by more than 150% for low-GI species. Increased proportional occurrences of the bRG lineage with increasing brain size was required to achieve estimates with $< 5\%$ deviation from observed neuron counts in all low-GI species (Table 2; Figure S7). Estimates of proportional occurrences in the mouse, marmoset, and rabbit are supported by previous work detailing relative abundances of different progenitor cell-types during cortical neurogenesis (Wang et al., 2011; Kelava et al., 2012), [IK and WBH, *in preparation*]. Evolutionary gain or loss of proliferative potential in the SVZ is an essential mechanistic determinant of neocortical expansion, such that its presence in high-GI species and absence in low-GI species is sufficient and even requisite for explaining neocortical evolution (Figure S8).

Adaptive evolution of proliferative potential in the basal germinal zone

To simulate the adaptiveness of evolving increased proliferative potential in the SVZ in two lissencephalic species - mouse and marmoset - we calculated trade-offs between neuroepithelial founder pool size and neurogenic period using mouse/marmoset and human programs of cortical neurogenesis to achieve one billion neurons. We show that, in both species, evolving a lineage of proliferating basal progenitors is between 2- and 6-times more cost-efficient than either expanding founder pool size or lengthening neurogenesis; and that the marmoset, by evolving proliferating progenitors, could keep its observed founder pool size or slightly reduce its neurogenic period to achieve one billion neurons (Figure S9). We further clarified the significance to neuronal output of each progenitor-type with deterministic and stochastic models of temporal dynamics and progenitor cell-type variables. From these we conclude that basal pro-

genitors are increasingly necessary in larger brains and that achieving 10^9 neurons is statistically implausible in the absence of proliferative basal progenitors (Table S4). Finally, we described the dynamics of asymmetric *versus* symmetric progenitors, isolated from their observed lineage beginning at the apical surface, by introducing three ordinary differential equations (ODEs) modeling a self-renewing cell that generates either a differentiated cell or proliferative cell. The ODEs describe a self-renewing mother progenitor, which can generate either a neuron or a proliferative daughter at each division. The proliferative daughter is allowed one proliferative division followed by self-consumption. The likelihood of a neuron or proliferative daughter being generated by the mother, therefore, is interdependent. We also include the pool of mother progenitors as a linear variable. We show that neuronal output of the system increases dramatically when both the initial pool of self-renewing cells and the likelihood of those initial cells to generate proliferative, rather than differentiated, cells approaches saturation (Figure S10).

Neurodevelopmental long intergenic non-coding RNA are selectively lost in low-GI species

In order to assess the degree to which morphological convergence is corroborated by convergence at the genomic level, we probed published RNA-seq data collected from human fetal neocortical germinal zones during mid-neurogenesis (Fietz et al., 2012). Because cis-acting non-coding RNAs proximal to genes differentially expressed in the human fetal brain show accelerated evolution along the human lineage, we limited our search to lincRNA. We identified 186 lincRNA differentially expressed in at least one germinal zone or the cortical plate (Table S8). Of these, we shortlisted 142, which had at least one adjacent protein-coding gene expressed during neurogenesis. We then determined whether the genes proximal to the lincRNA in the human genome (defined as the lincRNA gene neighborhood) were proximal to the same genomic sequence in 31 other species (30 mammals plus chicken). We found, firstly, that lincRNA gene-neighborhood conservation could not be explained by phylogenetic relatedness and that, secondly, gene-neighborhood conservation correlated well with GI ($R^2 = 0.68$, $P = 4.54 \times 10^{-6}$) and brain weight ($R^2 = 0.71$, $P = 4.55 \times 10^{-7}$), but poorly with maximum lifespan ($R^2 = 0.44$, $P = 0.0004$) and body weight ($R^2 = 0.39$, $P = 0.0001$). Furthermore, by calculating the number of lincRNA expected to be conserved in each species based on phylogenetic relatedness to human, we could determine which species fell below and which above null expectations. We found that all low-GI species (except the marmoset and manatee) fell below and all high-GI species above phylogenetic expectations. No such trend was found with lincRNA expressed maximally in adult adipose tissue (see *Determining the gene-neighborhood conservation of neurodevelop-*

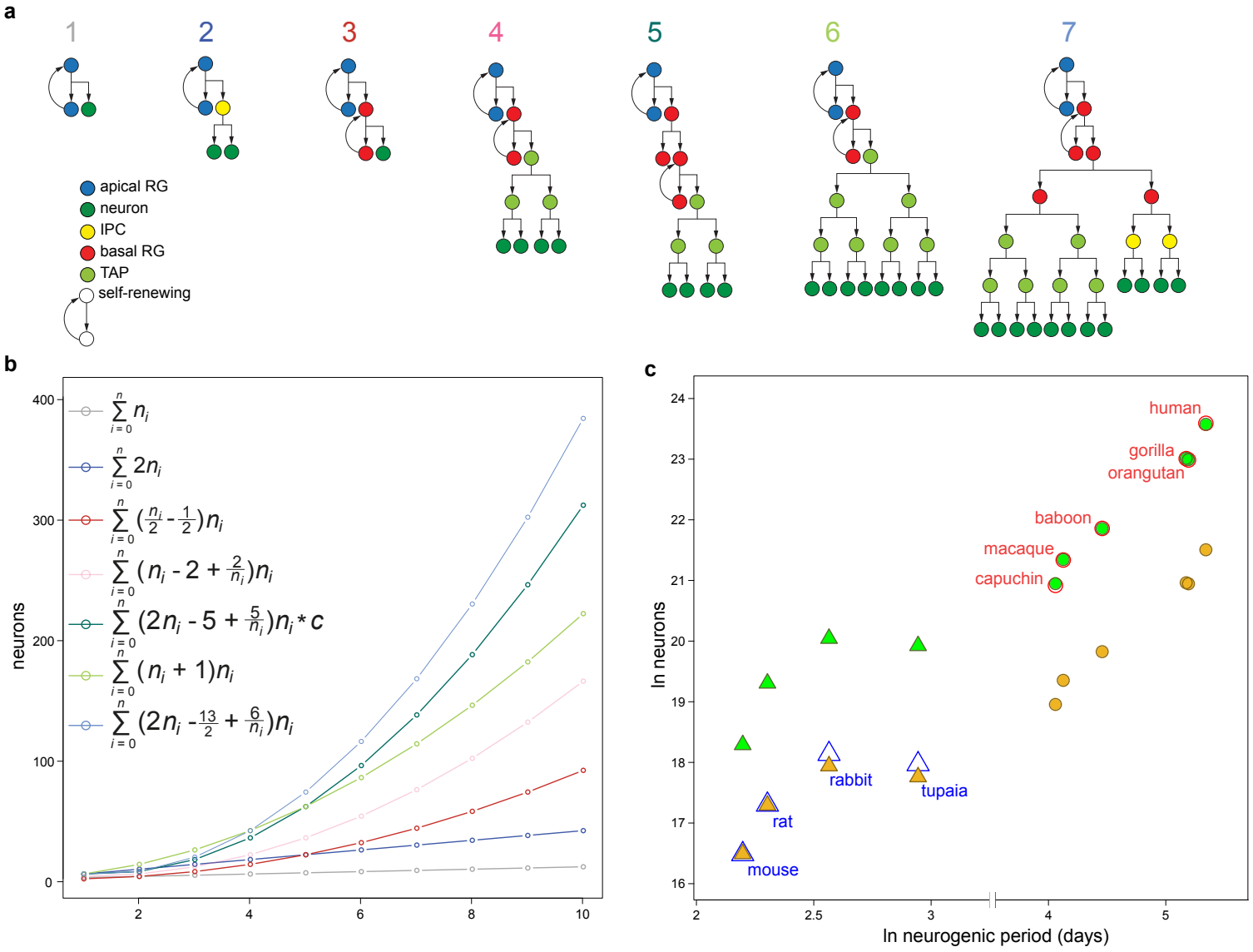

Figure 5: Distinct combinations of progenitor lineages are required to predict neocortical neuron numbers for low- *versus* high-GI species. (a) Schematics of the 7 lineages used to construct neurogenic output in species. (b) Plotted neuronal output of the lineages in (a) beginning with two cells, over 10 divisions. Series in the legend summarize the neuronal output of each lineage, where n_i is the number of i divisions. A constant, c = 0.989, is incorporated into the series for lineage 5, allowing the series to converge on the true value of the lineage output as the number of divisions becomes increasingly numerous. (c) Ln-transformed plot of observed neuron counts as a function of neurogenic period for 4 species with a GI $\leq$ 1.5 (open blue triangles) and 6 species with a GI $>$ 1.5 (open red circles). Predicted neuron counts were calculated using combinations of the lineages in (a) that accurately fitted to the observed neuron counts either for mouse (closed gold symbols) or human (closed green symbols). Note that the mouse neurogenic program implicates only lineages 1–3; the human neurogenic program only lineages 2–7; and that lineages 4–7 were considered interdependent, such that an increase (or decrease) in the occurrence of one of these lineages necessitated an attendant increase (or decrease) in the others. See Table 1 for observed and predicted neuron counts and Table 2 for the proportional contribution of each lineage for mouse and human.

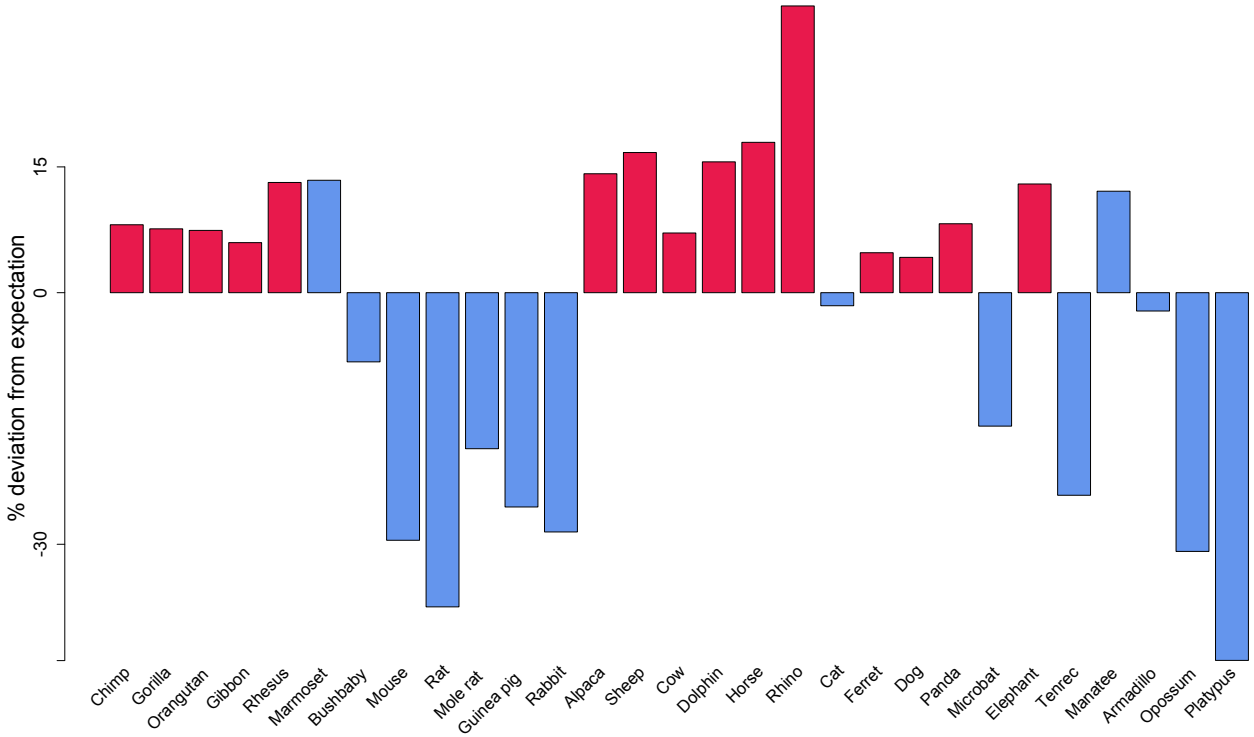

Figure 6: Gene-neighborhood conservation of 142 lincRNA expressed during human neurogenesis across 29 mammalian species. Conservation is shown to be above null phylogenetic expectations in high-GI species (red) and below expectations for low-GI species (blue). The two exceptions are the marmoset, a low-GI primate species, and the manatee, a large-brained lissencephalic species belong to Afrotheria; both of these show lincRNA gene-neighborhood conservation considerably above null expectations.

mental lincRNA). We therefore provide powerful evidence for a genomic correlate of the neuron threshold in the disproportionate conservation of neurodevelopmental lincRNA in high- *versus* low-GI species.

Discussion

The emergence of new structures, in the most general sense, is typically limited to selection on existing developmental processes; and conserved pathways may persist, over evolutionary time, even when the phenotype is transformed or unexpressed (Mayr, 1960; Shubin et al., 1997; Hall, 2003). However, it is also evident that development may be adapted without affecting phenotype (e.g., Bolker (1994); Kalinka and Tomancak (2012)). Therefore, in order to understand selective pressures acting on a discontinuous or convergent trait, it is necessary to investigate the underlying developmental processes generating it. We have shown that a gyrencephalic neocortex is ancestral to mammals, which is concordant with evidence (Romiguier et al., 2013) that the mammalian ancestor was large ($>$ 1kg) and long-lived ($>$ 25-year lifespan) and, furthermore, provides considerable resolution to recent evidence for a gyrencephalic eutherian ancestor (O'Leary et al., 2013) by sampling nearly twice as many species and categorizing gyrencephaly

as a continuous, rather than a binary, trait. More surprisingly, we show that convergent evolution of higher-orders of gyrencephaly along divergent lineages has been accompanied by two distinct constellations of physiological and life-history paradigms. Specifically, species with a GI > 1.5, which is commensurate with one billion cortical neurons, exhibit patterns of development and life-history that are distinct from species with a GI < 1.5, irrespective of phylogeny. This implies that there is a considerable constraint on either the ability of species of a given neocortical size to exploit certain ecologies or the potential for species of a given ecology to freely adapt neocortical size. Even marine mammals, whose selection pressures are *sui generis*, may largely be held to the same evolutionary stereotyping as terrestrial mammals (Figure S11). Furthermore, no species - with the exception of the house cat (*Felis catus*), which may be under unique selection pressures due to its ten-thousand-year-old domestication (Driscoll et al., 2009) - falls within the limits of the GI or neuronal threshold range (Figure 3d). While our results countenance previous studies showing associations between physiological and life-history traits in mammals (see Martin et al. (2005)), we identify those traits to have a bimodal distribution, rather than to vary allometrically, across species. This distribution depicts a Waddington-type landscape for neocortical expansion – albeit relevant at the species-level - wherein the threshold represents an adaptive peak requiring a particular adaptation in neurogenic programming within a population for traversal. Our results may explain this landscape by mechanistic differences occurring during cortical neurogenesis between species above and below the threshold: the necessity of proliferative basal progenitors in high-GI species and their putative absence in low-GI species. The adaptation of proliferative basal progenitors may be tantamount to a relaxation of constraints along lineages leading to larger-brained species (Boddy et al., 2012), however, our analysis of lincRNA gene-neighborhood conservation suggests that the selective loss of genomic elements regulating neurogenesis is responsible for the evolution of low-GI species. The loss of lincRNA in low-GI species, which are typically small-bodied (Figure 2a), may simply be caused by a higher rate of meiotic combination in low-GI species, resulting in more frequent meiotic errors and thereupon loss of lincRNA (Lewitus and Kalinka, 2013). But, firstly, this does not proscribe a functional role for lincRNA in the differential regulation of neurogenesis in low- *versus* high-GI species; and, secondly, both the greater predictive powers of GI and brain weight compared to lifespan or body weight for lincRNA gene-neighborhood conservation and the more strictly phylogenetic conservation of lincRNA gene-neighborhood for non-neurodevelopmental lincRNA (see *Neurodevelopmental long intergenic non-coding RNA are selectively lost in low-GI species*) speak in favor of the relevance of neocortical development for the selective loss or retention of certain lincRNA.

Furthermore, our human neurogenic program clearly shows that the same neurogenic lin-

eages in the same proportions are required to generate the neocortices of monkeys, apes, and humans, and may even be extended to carnivores, cetartiodactlys, and other high-GI species (Figure S11), demonstrating that neurogenic period alone may be sufficient to explain differences in neocortical size between any species in the same GI group (Figure S12).

We propose that proliferative basal progenitors, rather than simply an abundance of asymmetrically dividing bRGs in an expanded SVZ, are necessary and sufficient for the evolution of an expanded and highly folded neocortex in mammals. Recent work in the fetal macaque support this proposal (Betizeau et al., 2013). We thus conclude that an increase in proliferative potential in the basal neurogenic program is an adaptive requirement for traversing the evolutionary threshold identified here. But because we reconstruct the eutherian ancestor to have a GI value of 1.48 ± 0.13 (s.e.m.), which falls within the range of the observed threshold, we are left with an ambivalent evolutionary history for mammalian neocortical expansion: either (i) proliferative basal progenitors are ancestral to all eutherian mammals and were selected against along multiple lineages (e.g., rodents, strepsirrhines), so that the ultimate loss of basal proliferative potential in certain taxa, and therefore the evolution of low-GI species, is the result of divergent developmental adaptations; or (ii) proliferative basal progenitors are not ancestral to eutherian mammals, but evolved convergently along multiple lineages, in which case the developmental process for their inclusion in neurogenic programming may be conserved, even if that process was unexpressed for long stretches of mammalian evolution. While both of these histories are speculative, the prodigious conservation of lincRNA in high- *versus* low-GI species supports (i). Ultimately, we have revealed an important insight into mammalian evolution: a threshold exists in mammalian brain evolution; neocortical expansion beyond that threshold requires a specific class of progenitor cell-type, likely regulated by lincRNA; and the difference in neurogenic programming between any species on the same side of that threshold does not require novel progenitor-types or adaptations in progenitor-type behavior. Further experimental research into the conservation of genomic regions regulating the expression of proliferative basal progenitors, either at the ventricle or through maintenance of a proliferative niche in the SVZ, in low- *versus* high-GI species may be sufficient to determine whether the mechanism for neocortical expansion has evolved independently in distantly related species or is the product of a deep homology in mammalian neurogenesis.

Materials and Methods

Calculating GI

We calculated GI using images of Nissl-stained coronal sections from http://brainmuseum.org. We used 10-22 sections, equally spaced along the anterior-posterior axis of the brain, for each species (Figure S1). The inner and outer counters of the left hemisphere were traced in Fiji (http://fiji.sc/wiki/index.php/Fiji). The values calculated are marked with an asterisk in Table S1. Additional GI values were collected from the literature (Table S1; External Database 1). Species (e.g., platypus) whose cortical folding has been described (Goffinet, 2006; Rowe, 1990), but not measured according to the method established in Zilles et al. (1988), were omitted from our analyses (see *Reconstructing the evolutionary history of GI*). Work in humans and baboons has shown that inter-indvidual variation in GI is not enough to outweigh interspecific differences (Rogers et al., 2010; Toro et al., 2008).

Stochastic mapping of GI across the mammalian phylogeny

We used a comprehensive phylogenetic approach to map 41 life-history and physiological character traits collected from the literature (Tables S1,S2) onto hypotheses of phylogenetic relationships in Mammalia, in order to examine how those traits correlate, over evolutionary time, with degree of gyrencephaly. Continuous character traits were discretized using the consensus of natural distribution breaks calculated with a Jenks-Caspall algorithm (Jenks and Caspall, 1971), model-based clustering according to the Schwarz criterion (Fraley and Raftery, 2002), and hierarchical clustering (Szekely and Rizzo, 2005). Character histories were then corrected for body mass with a phylogenetic size correction (Collar and Wainwright, 2006) and summarized across the phylogeny using posterior probabilities. Associations between individual states of each character trait along those phylogenetic histories were calculated in SIMMAP (v1.5) using empirical priors (Bollback, 2006); the association between any two states was a measure of the frequency of occurrence (i.e., the amount of branch length across the tree) of those states on the phylogeny. The sums, rates, and types of changes for GI and body weight were plotted as mutational maps to assess directional biases in their evolution (Cunningham, 1999; Huelsenbeck and Rannala, 2003; Lewitus and Soligo, 2011). The phylogeny used in this analysis was derived from a species-level supertree (Bininda-Emonds et al., 2007). We appreciate that the phylogenetic hypothesis reconstructed by (Meredith et al., 2011) gives notably deeper divergence dates for mammalian subclasses, however, not enough of our sampled species were included in this reconstruction for it to be useful here.

Reconstructing the evolutionary history of GI

Variation in the mode and tempo of a continuous character trait is not always best characterized by a random walk (i.e., Brownian motion). Therefore, we compared a range of evolutionary models on the phylogenetic distribution of GI to find the best fit for the data (Felsenstein, 1973; Harmon et al., 2008; O'Meara et al., 2006; Paradis et al., 2004). Log-likelihood scores for each model were tried against the random walk score using the cumulative distribution function of the χ^2 distribution. Maximum-likelihood ancestral character states of GI and rate-shifts in the evolution of GI were then constructed using the best-fit model, with the standard error and confidence intervals calculated from root node reconstruction in PDAP using independent contrasts (Garland and Ives, 2000; Garland et al., 2005; Maddison and Maddison, 2011). Although a number of putatively lissencephalic non-eutherians were unavailable for our analyses (see *Calculating GI*), we nonetheless reconstructed alternative ancestral GI values that included one hypothetical monotreme and three hypothetical marsupials (Table S5). To trace evolutionary changes in GI at individual nodes and along lineages, we used a two-rate mode that highlighted the differences in high (> 1) *versus* low (< 1) root-to-tip substitutions and then sampled rates based on posterior probabilities across the tree using a Monte Carlo Markov Chain. We assumed that transitioning between adjacent GI values had the highest likelihood of occurrence. The rate at a given node could then be compared to the rate at the subsequent node to determine if a rate transition was likely. We corroborated these results using the *auteur* package (Eastman et al., 2011), which calculates rate-transitions at internal nodes under the assumption of an Ornstein-Uhlenbeck selection model (Butler and King, 2004) over one million Monte Carlo sampling iterations drawn from random samplings of posterior distributions of lineage-specific rates. Scaling relationships were determined for GI as a function of all continuous life-history and physiological traits, including adult cortical neuron counts. For three insectivore (*Sorex fumeus, Blarina brevicauda, Scalopus aquaticus*) species, data were available for neuron counts but not GI, and therefore we extrapolated the GI of those species based on gross morphology. Finally, to test whether the bimodal distribution of GI may be influenced by the topology of the mammalian phylogenetic tree, we used an expectation-maximization algorithm. Each simulated trait was given the same variance as GI (Figure S5) and the result was averaged over 10^4 simulated datasets. None of the simulations produced the same bimodal distribution of species observed for GI data.

Estimating neuroepithelial founder pool populations

We estimated neuroepithelial founder pool populations for mouse and human. For the mouse, we used coronal sections of an E11.5 mouse embryo obtained from the Allen Brain Atlas (Lein

et al., 2007). We obtained 19 sections equidistantly spaced along the anterior-posterior axis of the brain. The length of the ventricular surface of the dorsal telencephalon was manually traced in Fiji (Schindelin et al., 2012) on each section starting from the point above the nascent hippocampus and ending in the point above the lateral ganglionic eminence. The horizontal length of the embryonic brain at E11.5 was measured with images from (Bejerano et al., 2006). Using the coronal and horizontal measurements, we constructed a polygon representing the ventricular surface of the dorsal telencephalon and calculated the area of this surface in Fiji. We measured the surface area of the end-feet of neuroepithelial cells using EM images of the coronally cut apical surface of an E11.5 embryonic brain (Table S6). The diameter of a single cell was calculated by measuring the distance between the adherens junctions. We corroborated these end-feet calculations with published immunofluorescence stainings of the apical complex (ZO1 and N-cadherin) from an *en face* perspective (Bultje et al., 2009; Marthiens and ffrench-Constant, 2009). The average surface area of a single end-foot was calculated by approximating the end-foot as a hexagon; and the number of founder cells was estimated by dividing the surface of the dorsal telencephalon by the surface of an individual end-foot of the neuroepithelial cell, such that

$$\frac{Surface\ area(\mu m^2)}{2\pi(\frac{1}{2}Endfoot\ diameter(\mu m^2)}\frac{\sqrt{3}}{2} = founders \qquad (1)$$

Our final mouse values were comparable to those previously published (Haydar et al., 2000). For the human, we followed the same procedure, using 10 coronal sections and one horizontal section of a gestation week (GW) 9 brain (Bayer and Altman, 2006). End-feet were calculated using EM images of the apical surface of a human brain at GW13. The measurements are available in Table S6. Because the number of founder cells per surface area was nearly equivalent in mouse and human ($\sim$4 x 10^5/mm^2), we used this ratio, along with data on ventricular volume collected from the literature (Table S1; Table S2; External Database 1), to estimate neuroepithelial founder cell populations for a further 14 species (Table 1). For species where no data on ventricular volume were available, values were estimated based on a regression analysis against brain weight (Figure S6). Ventricular volume was then converted to surface area for each species by approximating the ventricle as a cylinder with a 4.5-to-1 height-to-diameter proportion. Ventricular volume-derived ventricular surface area estimates were corroborated with the surface areas calculated from the literature for mouse and human. Founder cell estimates were then computed based on the densities derived above for mouse and human. Using this method, but alternately ignoring our mouse and human calculations to define the parameters, we were able to predict mouse and human values within 10% of our calculations, respectively.

Mathematical modeling of neurogenesis

Workers have demonstrated the occurrence of three primary lineages of neuronal generation in mouse neurogenesis (Fietz and Huttner, 2011) and a further four lineages in human neurogenesis (Hansen et al., 2010). While there is evidence for at least one additional lineage in mouse (Noctor et al., 2004), and further lineages may be speculated, we limited our model to the seven that are considered to contribute most significantly to neuronal output (Rakic, 2009; Lui et al., 2011; Molnár, 2011; Betizeau et al., 2013). The sequence of neuron generation in each of these seven lineages was summarized in series and solved numerically (Figure 5b). Neurogenic period was either taken from the literature (External Database 1) or estimated based on a regression analysis of neurogenic period as a function of gestation period (Figure S6). Neurogenic period in human was estimated using empirical observations from the literature (Bystron et al., 2006; Howard et al., 2006; Malik et al., 2013). The averaged cell-cycle length for apical and basal progenitors from the mouse (18.5 hours) was used for all non-primates (Arai et al. (2011); Figure S13); averaged cell-cycle length for cortical areas 17 and 18 from the macaque (45 hours) was used for catarrhines (Lukaszewicz et al., 2005; Betizeau et al., 2013); and an intermediary cell-cycle length (30 hours), based on personal observations in marmoset, was used for platyrrhines. Diminishing numbers of neuroepithelial cells have been observed to continue to proliferate at the ventricle until E18.5 in the mouse (Haubensak et al., 2004). Therefore, final neuroepithelial founder pool estimates were calculated from the aforementioned by evenly decreasing the value of α in the Sherley equation (Sherley et al., 1995) from 1 at E9.5 to 0 at E18.5 in the mouse and at comparable neurogenic stages in other species. Neuron numbers were calculated for each species from combinations of lineages. The proportional contribution of each lineage for each species was parameterized according to existing data on progenitor cell-type abundances in mouse (Wang et al., 2011), marmoset (Kelava et al., 2012), rabbit [IK and WBH, *in preparation*], and macaque (Betizeau et al., 2013). Where no such data were available, proportional contributions were permutated for all lineages until a best-fit estimate, based on cortical neuron numbers taken from the literature (Azevedo et al., 2009; Gabi et al., 2010; Herculano-Houzel, 2010, 2011), was achieved (Tables 1,2). Each lineage was assumed to occur from the first to final day of neurogenesis, although this is only approximately accurate. Finally, because of published estimates of postnatal apoptosis in the mammalian cortex (Burek and Oppenheim, 1996; Hutchins and Barger, 1998; Bandeira et al., 2009), we assumed neuron counts to be 1.5-fold higher at the termination of neurogenesis than in the adult brain; therefore, neuron number at the termination of neurogenesis was estimated in each species by multiplying neuron numbers collected from the literature by 1.5. This multiplication is not represented in Table 1.

Calculating the effects of proliferative progenitors on neuronal output

Trade-offs in adapting a human neurogenic program with either an expanding neuroepithelial founder pool or lengthening neurogenic period were tested for the mouse (*Mus musculus*) and marmoset (*Callithrix jacchus*), two lissencephalic species whose cell-type proportions during neurogenesis have been documented (Noctor et al., 2004; Wang et al., 2011; Kelava et al., 2012). To estimate the relative reproductive value and stable-stage proportions of each of the lineages in the mouse and human neurogenic programs, we constructed a stage-structured Lefkovitch matrix, using sums of the lineage series (after 100 cycles) as fecundity values and complete permutations of the proportional contributions of each lineage as mortality values. The altered growth-rates of each lineage were calculated by excluding lineages one at a time and assuming 100% survival in the remaining lineages (Table S4). We introduced three ODEs to explore the average dynamics of asymmetric *versus* symmetric progenitors, such that: if a(t), b(t), and c(t) are the numbers of asymmetrically dividing cells, differentiated cells, and proliferative cells, respectively, then,

$$\frac{da}{dt} = 0 \tag{2}$$

$$\frac{db}{dt} = ra + 2rc \tag{3}$$

$$\frac{dc}{dt} = (1-r)a + (1-2r)c \tag{4}$$

where r is equal to growth-rate. If $a(t)$=a_0, then

$$b(t) = \frac{2r}{1-2r}(c_0 + \frac{1-r}{1-2r}a_0)(e^{(1-2r)t} - 1) - \frac{ra_0}{1-2r}t + b_0 \tag{5}$$

and

$$c(t) = (c_0 + \frac{1-r}{1-2r}a_0)e^{(1-2r)t} - \frac{ra_0}{1-2r}a_0 \tag{6}$$

We calculated the effect on neuronal output of increasing the likelihood of symmetrically dividing daughter progenitors in the lineage (Figure S10). The interdependent growth-rates in the model reflect a purely mechanistic interpretation of determining neuronal output from a finite pool of asymmetrically dividing cells. The ODEs, therefore, may not reflect differential regulation of neuronal output via direct *versus* indirect neurogenesis. The daughter proliferative cells are designed to carry out one round of proliferation followed by a final round of self-

consumption.

Determining the gene-neighborhood conservation of neurodevelopmental lincRNA

We used previously published RNA-seq data collected from the VZ, ISVZ, OSVZ, and cortical plate of human fetal neocortex at GW13–16 (Fietz et al., 2012) and employed the lincRNA discovery pipeline outlined by Cabili et al. (2011) to identify 186 lincRNA differentially expressed during human neocortical neurogenesis (Table S8). Of these, 161 were differentially upregulated in a germinal zone, including 43 overexpressed in the ISVZ and/or OSVZ compared to the VZ (Figure S14). Previous work has shown that sequence conservation is a poor predictor of functional conservation in non-coding RNA (Chodroff et al., 2010) and that long non-coding RNA are often functionally – or at least transcriptionally – linked to adjacently located protein-coding genes (Ponjavic et al., 2009). Therefore, for each lincRNA, we defined its gene neighborhood as the immediatly flanking protein-coding genes and discarded any lincRNA which did not have at least one flanking gene expressed during neurogenesis. The final list included 142 lincRNA, whose gene neighborhoods were collectively enriched for Gene Ontology terms related to forebrain development and cell proliferation (Table S9; Figure S15). We assessed lincRNA gene-neighborhood conservation for the 142 lincRNA in 32 species (chicken (Gallus gallus; galGal4), platypus (Ornithorhyncus anatinus; ornAna1), opossum (Monodelphis domestica; monDom5), armadillo (Dasyproctus novemcinctus; dasNov3), manatee (Trichechus manatus; triMan1), tenrec (Echinops telfari; echTel2), elephant (Loxodonta africana; loxAfr3), little brown bat (Myotis lucifugus; myoLuc2), giant panda (Ailuropoda melanoleuca; aliMel1), dog (Canis familiaris; canFam3), ferret (Mustela putorius furo; musFur1), cat (Felis catus; felCat5), white rhinoceros (Ceratotherium simum; cerSim1), horse (Equus caballus; equCab2), cow (Bos taurus; bosTau7), sheep (Ovis aries; oviAri3), dolphin (Tursiops truncatus; turTru2), alpaca (Vicugna pacos; vicPac2), rabbit (Oryctolagus cuniculus; oryCun2), guinea pig (Cavia porcellus; cavPor3), naked mole-rat (Heterocephalus glaber; hetGla2), rat (Rattus norvegicus; rn4), mouse (Mus musculus; mm10), bushbaby (Otolemur garnettii; otoGar3), marmoset (Callithrix jacchus; calJac3), baboon (Papio anubis; popAnu2), rhesus (macaca mulatta; rheMac3), gibbon (Nomascus leucogenys; nomLeu3), orangutan (Pongo pygmaeus abelii; ponAbe2), gorilla (Gorilla gorilla gorilla; gorGor3), chimpanzee (Pan troglodytes; panTro4), and human (Homo sapiens; hg19)) by BLASTing the lincRNA sequence retrieved from the human RNA-seq data and visually inspecting the gene-neighborhood for each species. To increase the likelihood of finding an orthologous region in the non-human species, we used both the entire lincRNA

sequence, as well as, when available, only the region of the lincRNA showing signs of transcriptional activity in human as evidenced by ENCODE data on chromatin-level information (Raney et al., 2011). Both sequences consistently identified the same region. Due to scaffolding, we were only able to assess a sample of the lincRNA (66) for the dolphin. After compiling the total conservation scores for each species (Table S9), where lincRNA gene-neighborhood could either be scored as conserved (1) or not conserved (0), we calculated expected scores for each species under an Ornstein-Uhlenbeck model based on phylogenetic generalized least squares (Grafen, 1989). The percentage deviations of actual from expected scores for each species are presented in Figure 6. PhyloP and PhastCons sequence conservation scores for primates were computed for lincRNA not conserved in mouse. Interestingly, for both metrics, sequence conservation scores were, on average, highest for gene-neighborhoods comprised by at least one transcription factor (Table S10; Figure S16).

Despite a significantly stronger correlation between lincRNA gene-neighborhood conservation and GI than lifespan, it remained a possibility that slower molecular rates of evolution in certain species could account for high rates of lincRNA conservation. However, both high- and low-GI species show rates of molecular evolution below the mammalian average (Bininda-Emonds, 2007) and there is no significant correlation between rate of molecular evolution and lincRNA gene-neighborhood conservation (R^2 = 0.001, P = 0.925). Furthermore, to determine whether lincRNA gene-neighborhood conservation tends to be higher in high- *versus* low-GI species for non-neurodevelopment-related lincRNA, we re-ran our analyses using lincRNA maximally expressed in human adipose tissue from Cabili et al. (2011). We show that the trend observed for neurodevelopment-related lincRNA does not extend to adipose tissue (Figure S17).

Acknowledgments: We would like to thank Michaela Wilsch-Bräuninger for providing electron microscopy data; Holger Brandl for help with the lincRNA pipeline; and Michael Hiller, Yannis Kalaidzidis, Fong Kuan Wong, and Alex Sykes for helpful comments on the manuscript; and EL would like to thank Evan Charles for helpful discussion. IK was a member of the International Max Planck Research School of Molecular Cell Biology and Bioengineering and a doctoral student at the Technische Universitat Dresden.

Table 1: Parameters for models of cortical neurogenesis°

Species	*Gestation period (d)*	*Neurogenic period (d)†*	*Observed Neurons*	*Neuroepithelial founder pool (cells)†*	*Cell-cycle length (hours)* ¶
Human	270	112	1.63E+10	3.10E+07	45
Gorilla	257	103*	9.10E+09	1.59E+07	45
Orangutan	260	104*	8.90E+09	1.16E+07	45
Macaque	166	60	1.71E+09	4.41E+06	45
Baboon	180	72*	2.88E+09	6.37E+06	45
Capuchin	158	59*	1.14E+09	2.97E+06	45
Owl monkey	138	55*	4.42E+08	1.05E+06	30
Callimico	153	60*	3.57E+08	6.92E+05	30
Marmoset	146	58	2.45E+08	6.71E+05	30
Galago	134	54*	2.26E+08	1.01E+06	30
Tupaia	46	19*	6.04E+07	5.68E+05	18.5
Rabbit	30	13	7.15E+07	8.08E+05	18.5
Agouti	112	45*	1.10E+08	9.80E+05	18.5
Capybara	137	55*	3.10E+08	1.78E+06	18.5
Rat	21	10	3.10E+07	5.40E+05	18.5
Mouse	19	9	1.37E+07	3.99E+05	18.5

°*see External Database 1*

†see Materials and Methods

**estimate based on regression against gestation period (see Figure S6*)

¶*see Materials and Methods and Figure S11.*

Table 2: Best-fit proportional occurrences (%) of lineages in different taxa[œ]

Taxa	Lineage 1	Lineage 2	Lineage 3	Lineage 4-7
Catarrhines	0	20	40	40
Capuchin	0	20	40	40
Owl monkey	0	50	50	0
Callimico	0	50	50	0
Marmoset[§]	0	60	40	0
Galago	0	75	25	0
Tupaia	10	75	15	0
Rabbit[§]	10	75	15	0
Agouti	10	75	15	0
Capybara	10	75	15	0
Rat	10	80	10	0
Mouse[§]	10	80	10	0

[§] *supported by observational data (see Materials and Methods)*

[œ]*see Figure 5*.

References

Arai, Y., Pulvers, J. N., Haffner, C., Schilling, B., Nüsslein, I., Calegari, F., and Huttner, W. B. (2011). Neural stem and progenitor cells shorten s-phase on commitment to neuron production. *Nature Communications*, 2:154. PMID: 21224845.

Azevedo, F. A. C., Carvalho, L. R. B., Grinberg, L. T., Farfel, J. M., Ferretti, R. E. L., Leite, R. E. P., Jacob Filho, W., Lent, R., and Herculano-Houzel, S. (2009). Equal numbers of neuronal and nonneuronal cells make the human brain an isometrically scaled-up primate brain. *The Journal of Comparative Neurology*, 513(5):532–541. PMID: 19226510.

Bandeira, F., Lent, R., and Herculano-Houzel, S. (2009). Changing numbers of neuronal and non-neuronal cells underlie postnatal brain growth in the rat. *Proceedings of the National Academy of Sciences of the United States of America*, 106(33):14108–14113. PMID: 19666520.

Bayer, S. A. and Altman, J. (2006). *Atlas of Human Central Nervous System Development: The human brain during the later first trimester*. CRC Press, Florida.

Bejerano, G., Lowe, C. B., Ahituv, N., King, B., Siepel, A., Salama, S. R., Rubin, E. M., Kent, W. J., and Haussler, D. (2006). A distal enhancer and an ultraconserved exon are derived from a novel retroposon. *Nature*, 441(7089):87–90. PMID: 16625209.

Betizeau, M., Cortay, V., Patti, D., Pfister, S., Gautier, E., Bellemin-Ménard, A., Afanassieff, M., Huissoud, C., Douglas, R. J., Kennedy, H., and Dehay, C. (2013). Precursor diversity and complexity of lineage relationships in the outer subventricular zone of the primate. *Neuron*, 80(2):442–457. PMID: 24139044.

Bininda-Emonds, O. R. P. (2007). Fast genes and slow clades: comparative rates of molecular evolution in mammals. *Evol. Bioinform. Online*, 3:59–85. PMID: 19461986.

Bininda-Emonds, O. R. P., Cardillo, M., Jones, K. E., MacPhee, R. D. E., Beck, R. M. D., Grenyer, R., Price, S. A., Vos, R. A., Gittleman, J. L., and Purvis, A. (2007). The delayed rise of present-day mammals. *Nature*, 446(7135):507–512. PMID: 17392779.

Boddy, A. M., McGowen, M. R., Sherwood, C. C., Grossman, L. I., Goodman, M., and Wildman, D. E. (2012). Comparative analysis of encephalization in mammals reveals relaxed constraints on anthropoid primate and cetacean brain scaling. *Journal of Evolutionary Biology*, 25(5):981–994.

Bolker, J. A. (1994). Comparison of gastrulation in frogs and fish. *American Zoologist*, 34(3):313 –322.

Bollback, J. P. (2006). SIMMAP: stochastic character mapping of discrete traits on phylogenies. *BMC Bioinformatics*, 7:88. PMID: 16504105.

Borrell, V. and Reillo, I. (2012). Emerging roles of neural stem cells in cerebral cortex development and evolution. *Developmental Neurobiology*, 72(7):955–971. PMID: 22684946.

Bultje, R. S., Castaneda-Castellanos, D. R., Jan, L. Y., Jan, Y., Kriegstein, A. R., and Shi, S. (2009). Mammalian par3 regulates progenitor cell asymmetric division via notch signaling in the developing neocortex. *Neuron*, 63(2):189–202.

Burek, M. J. and Oppenheim, R. W. (1996). Programmed cell death in the developing nervous system. *Brain Pathology*, 6(4):427–446. PMID: 8944315.

Butler, M. and King, A. (2004). Phylogenetic comparative analysis: a modeling approach for adaptive evolution. *The American Naturalist*, 164(6):683–695.

Bystron, I., Rakic, P., Molnár, Z., and Blakemore, C. (2006). The first neurons of the human cerebral cortex. *Nature Neuroscience*, 9(7):880–886. PMID: 16783367.

Cabili, M. N., Trapnell, C., Goff, L., Koziol, M., Tazon-Vega, B., Regev, A., and Rinn, J. L. (2011). Integrative annotation of human large intergenic noncoding RNAs reveals global properties and specific subclasses. *Genes Dev.*, 25(18):1915–1927. PMID: 21890647.

Chodroff, R. A., Goodstadt, L., Sirey, T. M., Oliver, P. L., Davies, K. E., Green, E. D., Molnár, Z., and Ponting, C. P. (2010). Long noncoding RNA genes: conservation of sequence and brain expression among diverse amniotes. *Genome Biol.*, 11(7):R72. PMID: 20624288.

Collar, D. C. and Wainwright, P. C. (2006). Discordance between morphological and mechanical diversity in the feeding mechanism of centrarchid fishes. *Evolution*, 60(12):2575–2584. PMID: 17263118.

Collins, C. E., Airey, D. C., Young, N. A., Leitch, D. B., and Kaas, J. H. (2010). Neuron densities vary across and within cortical areas in primates. *Proc. Natl. Acad. Sci. U.S.A.*, 107(36):15927–15932. PMID: 20798050.

Cunningham, C. (1999). Some limitations of ancestral Character-State reconstruction when testing evolutionary hypotheses. *Systematic Biology*, 48:665–674.

Driscoll, C. A., Clutton-Brock, J., Kitchener, A. C., and O'Brien, S. J. (2009). The taming of the cat. genetic and archaeological findings hint that wildcats became housecats earlier–and in a different place–than previously thought. *Scientific American*, 300(6):68–75. PMID: 19485091.

Eastman, J. M., Alfaro, M. E., Joyce, P., Hipp, A. L., and Harmon, L. J. (2011). A novel comparative method for identifying shifts in the rate of character evolution on trees. *Evolution*, 65(12):3578–3589. PMID: 22133227.

Felsenstein, J. (1973). Maximum-likelihood estimation of evolutionary trees from continuous characters. *American Journal of Human Genetics*, 25(5):471–492. PMID: 4741844.

Fietz, S. A. and Huttner, W. B. (2011). Cortical progenitor expansion, self-renewal and neurogenesis-a polarized perspective. *Current Opinion in Neurobiology*, 21(1):23–35. PMID: 21036598.

Fietz, S. A., Kelava, I., Vogt, J., Wilsch-Bräuninger, M., Stenzel, D., Fish, J. L., Corbeil, D., Riehn, A., Distler, W., Nitsch, R., and Huttner, W. B. (2010). OSVZ progenitors of human and ferret neocortex are epithelial-like and expand by integrin signaling. *Nature Neuroscience*, 13(6):690–699. PMID: 20436478.

Fietz, S. A., Lachmann, R., Brandl, H., Kircher, M., Samusik, N., Schröder, R., Lakshmanaperumal, N., Henry, I., Vogt, J., Riehn, A., Distler, W., Nitsch, R., Enard, W., Pääbo, S., and Huttner, W. B. (2012). Transcriptomes of germinal zones of human and mouse fetal neocortex suggest a role of extracellular matrix in progenitor self-renewal. *Proceedings of the National Academy of Sciences of the United States of America*, 109(29):11836–11841. PMID: 22753484.

Finlay, B. L. and Darlington, R. B. (1995). Linked regularities in the development and evolution of mammalian brains. *Science*, 268(5217):1578–1584. PMID: 7777856.

Fraley, C. and Raftery, A. (2002). Model-Based clustering, discriminant analysis, and density estimation. *Journal of the American Statistical Association*, 97:611–631.

Franco, S. J. and Müller, U. (2013). Shaping our minds: stem and progenitor cell diversity in the mammalian neocortex. *Neuron*, 77(1):19–34. PMID: 23312513.

Gabi, M., Collins, C. E., Wong, P., Torres, L. B., Kaas, J. H., and Herculano-Houzel, S. (2010). Cellular scaling rules for the brains of an extended number of primate species. *Brain, Behavior and Evolution*, 76:32–44.

García-Moreno, F., Vasistha, N. A., Trevia, N., Bourne, J. A., and Molnár, Z. (2012). Compartmentalization of cerebral cortical germinal zones in a lissencephalic primate and gyrencephalic rodent. *Cerebral Cortex*, 22(2):482–492. PMID: 22114081.

Garland, Theodore, J., Bennett, A. F., and Rezende, E. L. (2005). Phylogenetic approaches in comparative physiology. *The Journal of Experimental Biology*, 208(Pt 16):3015–3035. PMID: 16081601.

Garland, Theodore, J. and Ives (2000). Using the past to predict the present: Confidence intervals for regression equations in phylogenetic comparative methods. *The American Naturalist*, 155(3):346–364. PMID: 10718731.

Goffinet, A. (2006). What makes us human? a biased view from the perspective of comparative embryology and mouse genetics. *Journal of Biomedical Discovery and Collaboration*, 1(1):16.

Grafen, A. (1989). The phylogenetic regression. *Philosophical Transactions of the Royal Society of London. B, Biological Sciences*, 326(1233):119–157.

Hager, R., Lu, L., Rosen, G. D., and Williams, R. W. (2012). Genetic architecture supports mosaic brain evolution and independent brain-body size regulation. *Nature Communications*, 3:1079. PMID: 23011133.

Hall, B. K. (2003). Descent with modification: the unity underlying homology and homoplasy as seen through an analysis of development and evolution. *Biological Reviews of the Cambridge Philosophical Society*, 78(3):409–433. PMID: 14558591.

Hansen, D. V., Lui, J. H., Parker, P. R. L., and Kriegstein, A. R. (2010). Neurogenic radial glia in the outer subventricular zone of human neocortex. *Nature*, 464(7288):554–561. PMID: 20154730.

Harmon, L. J., Weir, J. T., Brock, C. D., Glor, R. E., and Challenger, W. (2008). GEIGER: investigating evolutionary radiations. *Bioinformatics*, 24(1):129–131. PMID: 18006550.

Haubensak, W., Attardo, A., Denk, W., and Huttner, W. B. (2004). Neurons arise in the basal neuroepithelium of the early mammalian telencephalon: a major site of neurogenesis. *Proceedings of the National Academy of Sciences of the United States of America*, 101(9):3196–3201. PMID: 14963232.

Haydar, T. F., Nowakowski, R. S., Yarowsky, P. J., and Krueger, B. K. (2000). Role of founder cell deficit and delayed neuronogenesis in microencephaly of the trisomy 16 mouse. *The Journal of Neuroscience*, 20(11):4156 –4164.

Herculano-Houzel (2010). Coordinated scaling of cortical and cerebellar numbers of neurons. *Frontiers in Neuroanatomy*, 4(12).

Herculano-Houzel, S. (2011). Not all brains are made the same: new views on brain scaling in evolution. *Brain, Behavior and Evolution*, 78(1):22–36. PMID: 21691045.

Howard, B., Chen, Y., and Zecevic, N. (2006). Cortical progenitor cells in the developing human telencephalon. *Glia*, 53(1):57–66. PMID: 16158418.

Huelsenbeck, J. P. and Rannala, B. (2003). Detecting correlation between characters in a comparative analysis with uncertain phylogeny. *Evolution*, 57(6):1237–1247. PMID: 12894932.

Hutchins, J. B. and Barger, S. W. (1998). Why neurons die: cell death in the nervous system. *The Anatomical Record*, 253(3):79–90. PMID: 9700393.

Jenks, G. and Caspall, F. (1971). Error on choroplethic maps: definition, measurement, reduction. *Annals of the Association of American Geographers*, 61:217–244.

Kalinka, A. T. and Tomancak, P. (2012). The evolution of early animal embryos: conservation or divergence? *Trends in Ecology & Evolution*, 27(7):385–393. PMID: 22520868.

Kelava, I., Reillo, I., Murayama, A. Y., Kalinka, A. T., Stenzel, D., Tomancak, P., Matsuzaki, F., Lebrand, C., Sasaki, E., Schwamborn, J. C., Okano, H., Huttner, W. B., and Borrell, V. (2012). Abundant occurrence of basal radial glia in the subventricular zone of embryonic neocortex of a lissencephalic primate, the common marmoset callithrix jacchus. *Cerebral Cortex*, 22(2):469–481. PMID: 22114084.

Krubitzer, L. and Kaas, J. (2005). The evolution of the neocortex in mammals: how is phenotypic diversity generated? *Current Opinion in Neurobiology*, 15(4):444–453. PMID: 16026978.

Lein, E. S., Hawrylycz, M. J., Ao, N., Ayres, M., Bensinger, A., Bernard, A., Boe, A. F., Boguski, M. S., Brockway, K. S., Byrnes, E. J., Chen, L., Chen, L., Chen, T., Chin, M. C., Chong, J., Crook, B. E., Czaplinska, A., Dang, C. N., Datta, S., Dee, N. R., Desaki, A. L.,

Desta, T., Diep, E., Dolbeare, T. A., Donelan, M. J., Dong, H., Dougherty, J. G., Duncan, B. J., Ebbert, A. J., Eichele, G., Estin, L. K., Faber, C., Facer, B. A., Fields, R., Fischer, S. R., Fliss, T. P., Frensley, C., Gates, S. N., Glattfelder, K. J., Halverson, K. R., Hart, M. R., Hohmann, J. G., Howell, M. P., Jeung, D. P., Johnson, R. A., Karr, P. T., Kawal, R., Kidney, J. M., Knapik, R. H., Kuan, C. L., Lake, J. H., Laramee, A. R., Larsen, K. D., Lau, C., Lemon, T. A., Liang, A. J., Liu, Y., Luong, L. T., Michaels, J., Morgan, J. J., Morgan, R. J., Mortrud, M. T., Mosqueda, N. F., Ng, L. L., Ng, R., Orta, G. J., Overly, C. C., Pak, T. H., Parry, S. E., Pathak, S. D., Pearson, O. C., Puchalski, R. B., Riley, Z. L., Rockett, H. R., Rowland, S. A., Royall, J. J., Ruiz, M. J., Sarno, N. R., Schaffnit, K., Shapovalova, N. V., Sivisay, T., Slaughterbeck, C. R., Smith, S. C., Smith, K. A., Smith, B. I., Sodt, A. J., Stewart, N. N., Stumpf, K., Sunkin, S. M., Sutram, M., Tam, A., Teemer, C. D., Thaller, C., Thompson, C. L., Varnam, L. R., Visel, A., Whitlock, R. M., Wohnoutka, P. E., Wolkey, C. K., Wong, V. Y., Wood, M., Yaylaoglu, M. B., Young, R. C., Youngstrom, B. L., Yuan, X. F., Zhang, B., Zwingman, T. A., and Jones, A. R. (2007). Genome-wide atlas of gene expression in the adult mouse brain. *Nature*, 445(7124):168–176. PMID: 17151600.

Lewitus, E. and Kalinka, A. T. (2013). Neocortical development as an evolutionary platform for intragenomic conflict. *Frontiers in Neuroanatomy*, 7(2). PMID: 23576960.

Lewitus, E., Kelava, I., and Huttner, W. B. (2013). Conical expansion of the outer subventricular zone and the role of neocortical folding in evolution and development. *Front Hum Neurosci*, 7:424. PMID: 23914167.

Lewitus, E. and Soligo, C. (2011). Life-History correlates of placental structure in eutherian evolution. *Evolutionary Biology*, 38(3):287–305.

Lui, J. H., Hansen, D. V., and Kriegstein, A. R. (2011). Development and evolution of the human neocortex. *Cell*, 146(1):18–36.

Lukaszewicz, A., Savatier, P., Cortay, V., Giroud, P., Huissoud, C., Berland, M., Kennedy, H., and Dehay, C. (2005). G1 phase regulation, area-specific cell cycle control, and cytoarchitectonics in the primate cortex. *Neuron*, 47(3):353–364. PMID: 16055060.

Maddison, W. and Maddison, D. (2011). Mesquite: a modular system for evolutionary analysis.

Malik, S., Vinukonda, G., Vose, L. R., Diamond, D., Bhimavarapu, B. B. R., Hu, F., Zia, M. T., Hevner, R., Zecevic, N., and Ballabh, P. (2013). Neurogenesis continues in the third trimester of pregnancy and is suppressed by premature birth. *Journal of Neuroscience*, 33(2):411–423. PMID: 23303921.

Marthiens, V. and ffrench-Constant, C. (2009). Adherens junction domains are split by asymmetric division of embryonic neural stem cells. *EMBO reports*, 10(5):515–520. PMID: 19373255.

Martin, R. D., Genoud, M., and Hemelrijk, C. K. (2005). Problems of allometric scaling analysis: examples from mammalian reproductive biology. *The Journal of Experimental Biology*, 208(Pt 9):1731–1747. PMID: 15855404.

Mayr, E. (1960). The emegergence of evolutionary novelties. In *Evolution After Darwin*, pages 349–360. University of Chicago.

Meredith, R. W., Janečka, J. E., Gatesy, J., Ryder, O. A., Fisher, C. A., Teeling, E. C., Goodbla, A., Eizirik, E., Simão, T. L. L., Stadler, T., Rabosky, D. L., Honeycutt, R. L., Flynn, J. J., Ingram, C. M., Steiner, C., Williams, T. L., Robinson, T. J., Burk-Herrick, A., Westerman, M., Ayoub, N. A., Springer, M. S., and Murphy, W. J. (2011). Impacts of the cretaceous terrestrial revolution and KPg extinction on mammal diversification. *Science*, 334(6055):521–524. PMID: 21940861.

Miyata, T., Kawaguchi, A., Saito, K., Kawano, M., Muto, T., and Ogawa, M. (2004). Asymmetric production of surface-dividing and non-surface-dividing cortical progenitor cells. *Development*, 131(13):3133–3145. PMID: 15175243.

Molnár, Z. (2011). Evolution of cerebral cortical development. *Brain, Behavior and Evolution*, 78(1):94–107. PMID: 21691047.

Noctor, S. C., Flint, A. C., Weissman, T. A., Dammerman, R. S., and Kriegstein, A. R. (2001). Neurons derived from radial glial cells establish radial units in neocortex. *Nature*, 409(6821):714–720. PMID: 11217860.

Noctor, S. C., Martínez-Cerdeño, V., Ivic, L., and Kriegstein, A. R. (2004). Cortical neurons arise in symmetric and asymmetric division zones and migrate through specific phases. *Nature Neuroscience*, 7:136–144.

O'Leary, M. A., Bloch, J. I., Flynn, J. J., Gaudin, T. J., Giallombardo, A., Giannini, N. P., Goldberg, S. L., Kraatz, B. P., Luo, Z., Meng, J., Ni, X., Novacek, M. J., Perini, F. A., Randall, Z. S., Rougier, G. W., Sargis, E. J., Silcox, M. T., Simmons, N. B., Spaulding, M., Velazco, P. M., Weksler, M., Wible, J. R., and Cirranello, A. L. (2013). The placental mammal ancestor and the Post–K-Pg radiation of placentals. *Science*, 339(6120):662 –667.

O'Meara, B. C., Ané, C., Sanderson, M. J., and Wainwright, P. C. (2006). Testing for different rates of continuous trait evolution using likelihood. *Evolution*, 60(5):922–933. PMID: 16817533.

Pagel, M. (1999). Inferring the historical patterns of biological evolution. *Nature*, 401(6756):877–884. PMID: 10553904.

Paradis, E., Claude, J., and Strimmer, K. (2004). APE: analyses of phylogenetics and evolution in r language. *Bioinformatics*, 20(2):289–290. PMID: 14734327.

Pillay, P. and Manger, P. R. (2007). Order-specific quantitative patterns of cortical gyrification. *European Journal of Neuroscience*, 25(9):2705–2712.

Ponjavic, J., Oliver, P. L., Lunter, G., and Ponting, C. P. (2009). Genomic and transcriptional co-localization of protein-coding and long non-coding RNA pairs in the developing brain. *PLoS Genet.*, 5(8):e1000617. PMID: 19696892.

Rakic, P. (2009). Evolution of the neocortex: a perspective from developmental biology. *Nature Reviews Neuroscience*, 10(10):724–735. PMID: 19763105.

Raney, B. J., Cline, M. S., Rosenbloom, K. R., Dreszer, T. R., Learned, K., Barber, G. P., Meyer, L. R., Sloan, C. A., Malladi, V. S., Roskin, K. M., Suh, B. B., Hinrichs, A. S., Clawson, H., Zweig, A. S., Kirkup, V., Fujita, P. A., Rhead, B., Smith, K. E., Pohl, A., Kuhn, R. M., Karolchik, D., Haussler, D., and Kent, W. J. (2011). ENCODE whole-genome data in the UCSC genome browser (2011 update). *Nucleic Acids Res.*, 39(Database issue):D871–875. PMID: 21037257.

Reillo, I., de Juan Romero, C., García-Cabezas, M. Á., and Borrell, V. (2011). A role for intermediate radial glia in the tangential expansion of the mammalian cerebral cortex. *Cerebral Cortex*, 21(7):1674–1694. PMID: 21127018.

Rogers, J., Kochunov, P., Zilles, K., Shelledy, W., Lancaster, J., Thompson, P., Duggirala, R., Blangero, J., Fox, P. T., and Glahn, D. C. (2010). On the genetic architecture of cortical folding and brain volume in primates. *Neuroimage*, 53(3):1103–1108. PMID: 20176115.

Romiguier, J., Ranwez, V., Douzery, E. J. P., and Galtier, N. (2013). Genomic evidence for large, long-lived ancestors to placental mammals. *Molecular Biology and Evolution*, 30(1):5–13. PMID: 22949523.

Rowe, M. (1990). Organisation of the cerebral cortex in monotremes and marsupials. In Jones, E. and A, P., editors, *Comparative structure and Evolution of Cerebral Cortex, Part II*, volume 8B of *Cerebral Cortex*, pages 163–334. Plenum, New York.

Schindelin, J., Arganda-Carreras, I., Frise, E., Kaynig, V., Longair, M., Pietzsch, T., Preibisch, S., Rueden, C., Saalfeld, S., Schmid, B., Tinevez, J., White, D. J., Hartenstein, V., Eliceiri, K., Tomancak, P., and Cardona, A. (2012). Fiji: an open-source platform for biological-image analysis. *Nature Methods*, 9(7):676–682. PMID: 22743772.

Sherley, J. L., Stadler, P. B., and Stadler, J. S. (1995). A quantitative method for the analysis of mammalian cell proliferation in culture in terms of dividing and non-dividing cells. *Cell Proliferation*, 28:137–144.

Shitamukai, A., Konno, D., and Matsuzaki, F. (2011). Oblique radial glial divisions in the developing mouse neocortex induce self-renewing progenitors outside the germinal zone that resemble primate outer subventricular zone progenitors. *The Journal of Neuroscience*, 31(10):3683–3695. PMID: 21389223.

Shubin, N., Tabin, C., and Carroll, S. (1997). Fossils, genes and the evolution of animal limbs. *Nature*, 388(6643):639–648. PMID: 9262397.

Smart, I. H. M., Dehay, C., Giroud, P., Berland, M., and Kennedy, H. (2002). Unique morphological features of the proliferative zones and postmitotic compartments of the neural epithelium giving rise to striate and extrastriate cortex in the monkey. *Cerebral Cortex*, 12(1):37–53. PMID: 11734531.

Szekely, G. and Rizzo, M. (2005). Hierarchical clustering via joint Between-Within distances: Extending ward's minimum variance method. *Journal of Classification*, 22:151–183.

Toro, R., Perron, M., Pike, B., Richer, L., Veillette, S., Pausova, Z., and Paus, T. (2008). Brain size and folding of the human cerebral cortex. *Cerebral Cortex*, 18(10):2352 –2357.

Wang, X., Tsai, J., LaMonica, B., and Kriegstein, A. R. (2011). A new subtype of progenitor cell in the mouse embryonic neocortex. *Nature Neuroscience*, 14(5):555–561.

Young, N. A., Collins, C. E., and Kaas, J. H. (2013). Cell and neuron densities in the primary motor cortex of primates. *Front Neural Circuits*, 7:30. PMID: 23450743.

Zilles, K., Armstrong, E., Schleicher, A., and Kretschmann, H. J. (1988). The human pattern of gyrification in the cerebral cortex. *Anat. Embryol.*, 179(2):173–179. PMID: 3232854.

Zilles, K., Palomero-Gallagher, N., and Amunts, K. (2013). Development of cortical folding during evolution and ontogeny. *Trends in Neurosciences*. PMID: 23415112.

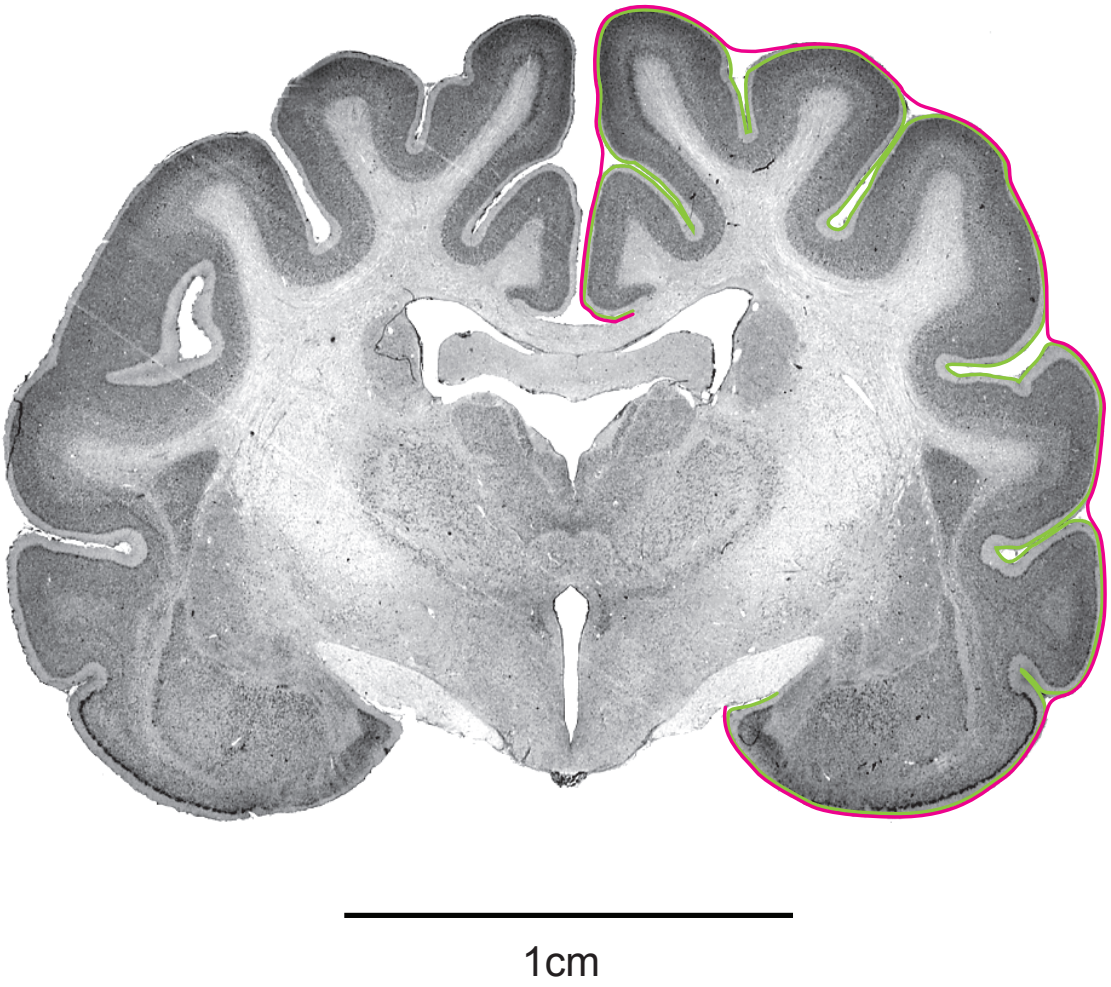

Figure S1: Coronal section of the brain of an adult house cat (*Felis catus*) (obtained from www.brainmuseum.org) illustrating the method used to calculate GI values as described in Zilles et al. (1988). Green line, actual contour; magenta line, hypothetical outer contour.

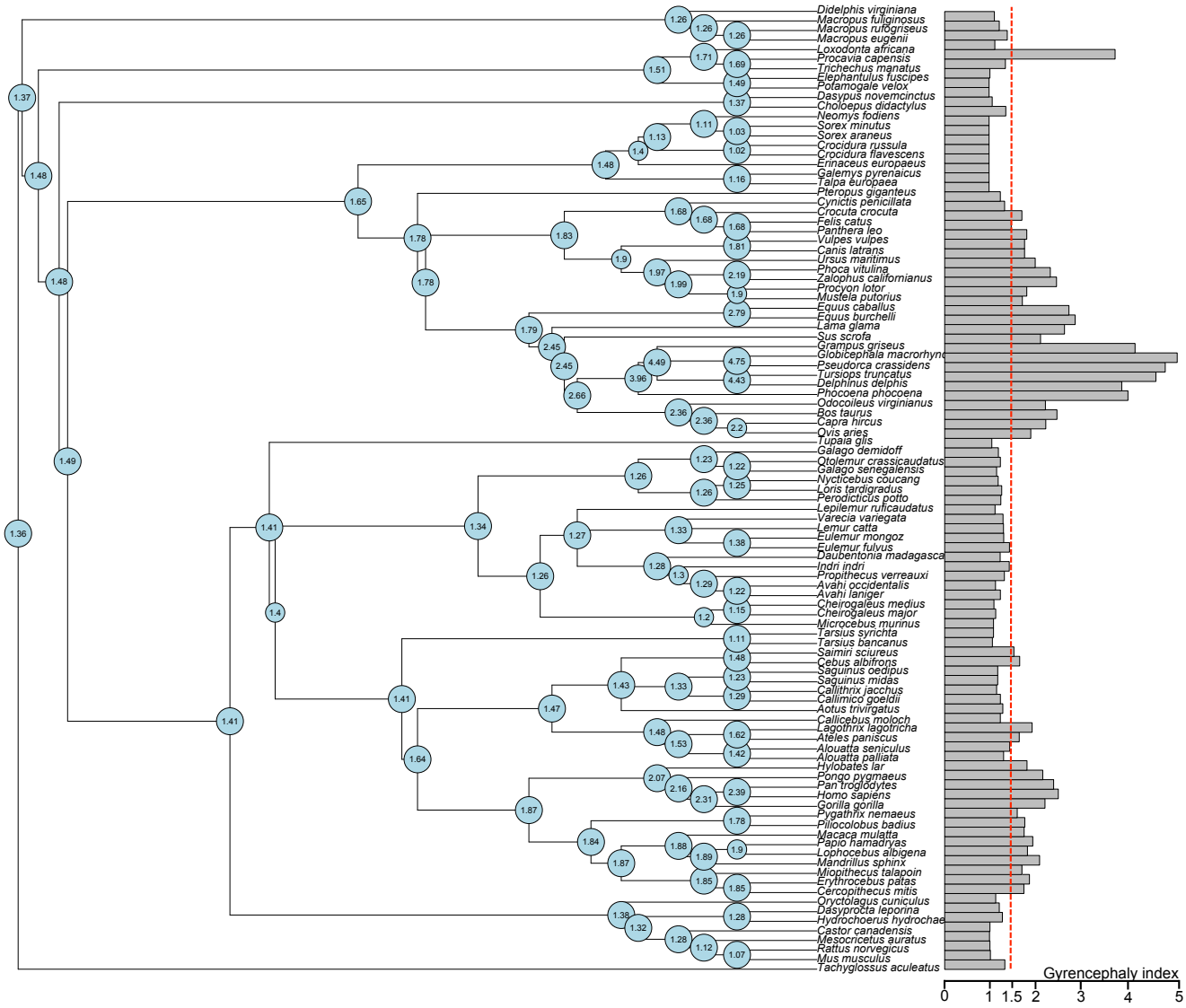

Figure S2: Maximum-likelihood ancestral node reconstruction of GI values at all internal nodes based on a delta ($\delta = 2.635$) selection model. Barplot shows the distribution of GI values across the phylogeny; dashed red line indicates GI = 1.5.

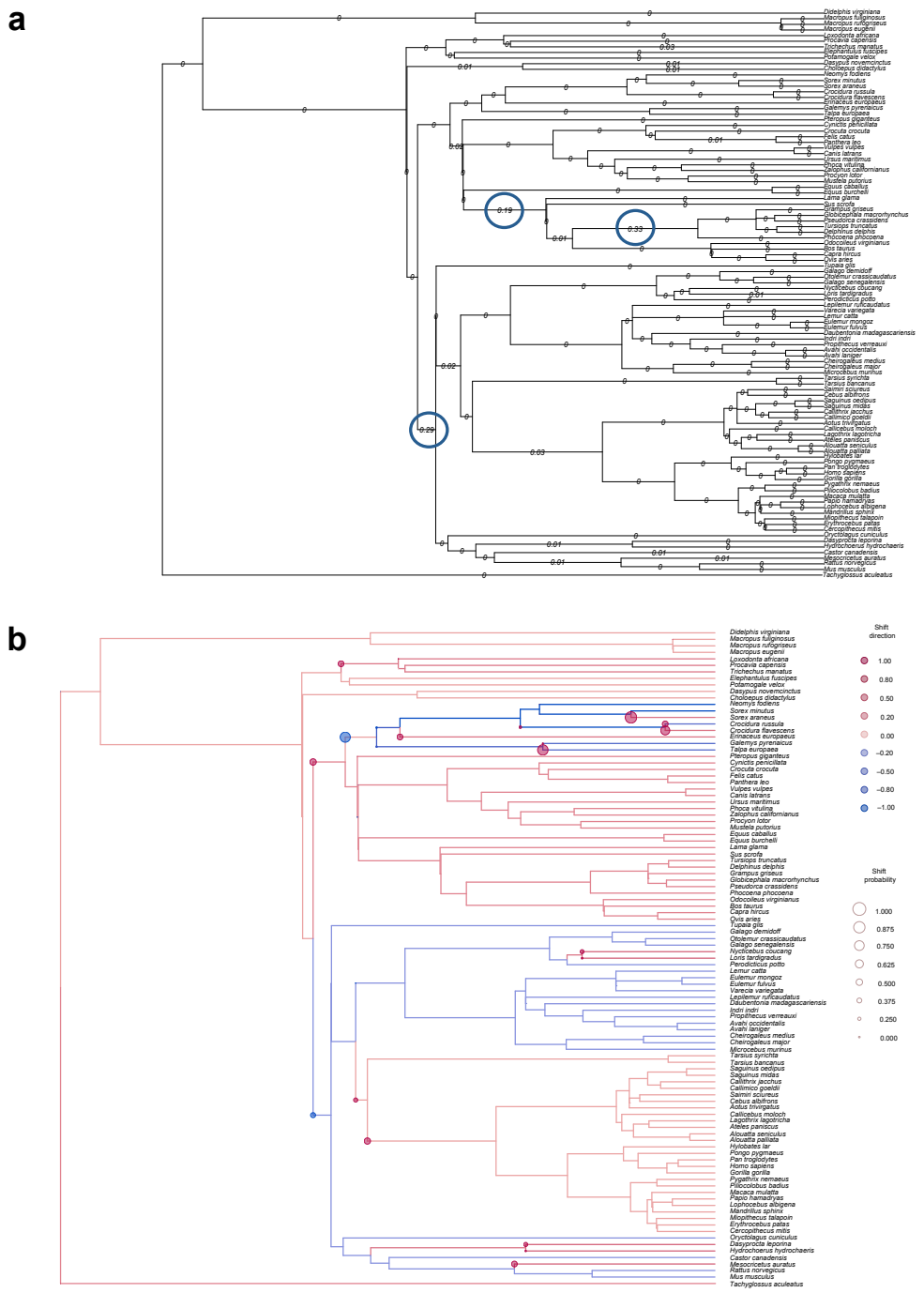

Figure S3: Rate-transitions in the mutation rate of GI values along lineages of the mammalian phylogeny. (a) A two-mode selection model that weights low over high root-to-tip substitutions. Numbers on the branches indicate the change in mutation-rate compared to the previous branch; 0 values indicate no significant change, values > 0 indicate significant change ($P < 0.05$). Note the especially high rate-transitions leading to primates, cetartiodactyls, and cetaceans (open blue circles). (b) Mutation- and transition-rate estimates of GI values using an Ornstein-Uhlenbeck selection model. Branches are colored to illustrate whether the mutation-rate estimates along each lineage are above (red) or below (blue) the median rate (orange); nodes are circled to indicate the posterior support of a transition-rate-shift event. The gradient of colors (see key) indicates the degree of deviation of the mutation-rate estimates (branches) and transition-rate estimates (nodes) from the median, with the highest deviation being arbitrarily set to $\pm$ 1.0 and the median to 0.0; the size of the circles (see key) at the nodes indicates the degree of posterior support for a transition-rate-shift event, with the highest value being arbitrarily set to 1.0 and lack of support to 0.0. Note that simians have evolved GI values at a rate consistent with the mammalian median.

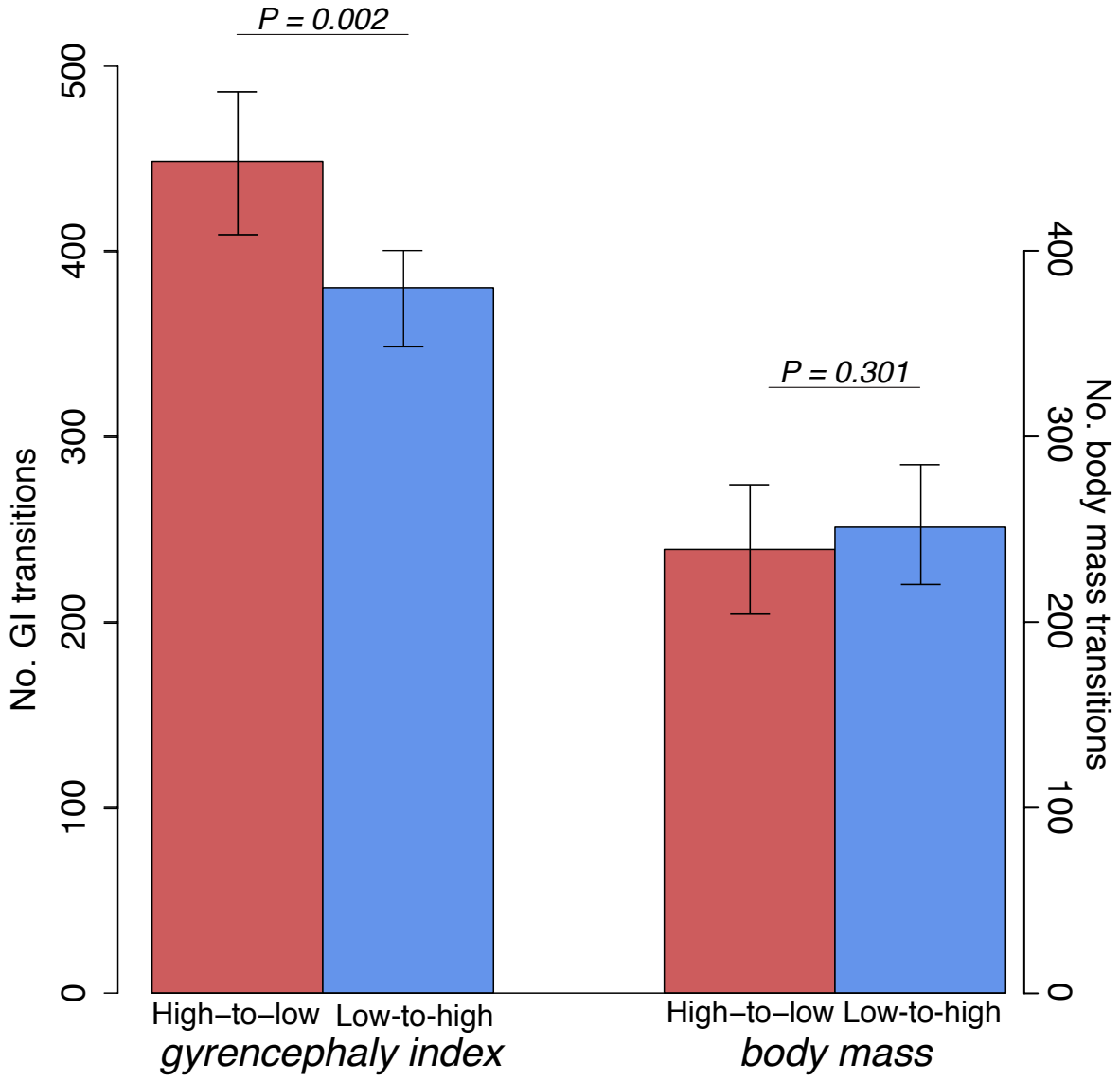

Figure S4: Barplots of types of transitions over mammalian evolution between four GI groups (see Figure 2a) and between five body mass groups averaged over 10^5 simulations. The number of total transitions from one GI or body mass group to another is summed as either high-to-low or low-to-high transitions. Note that significantly more high-to-low than low-to-high transitions are observed for GI, but that no significant difference in type of transition is observed for body mass.

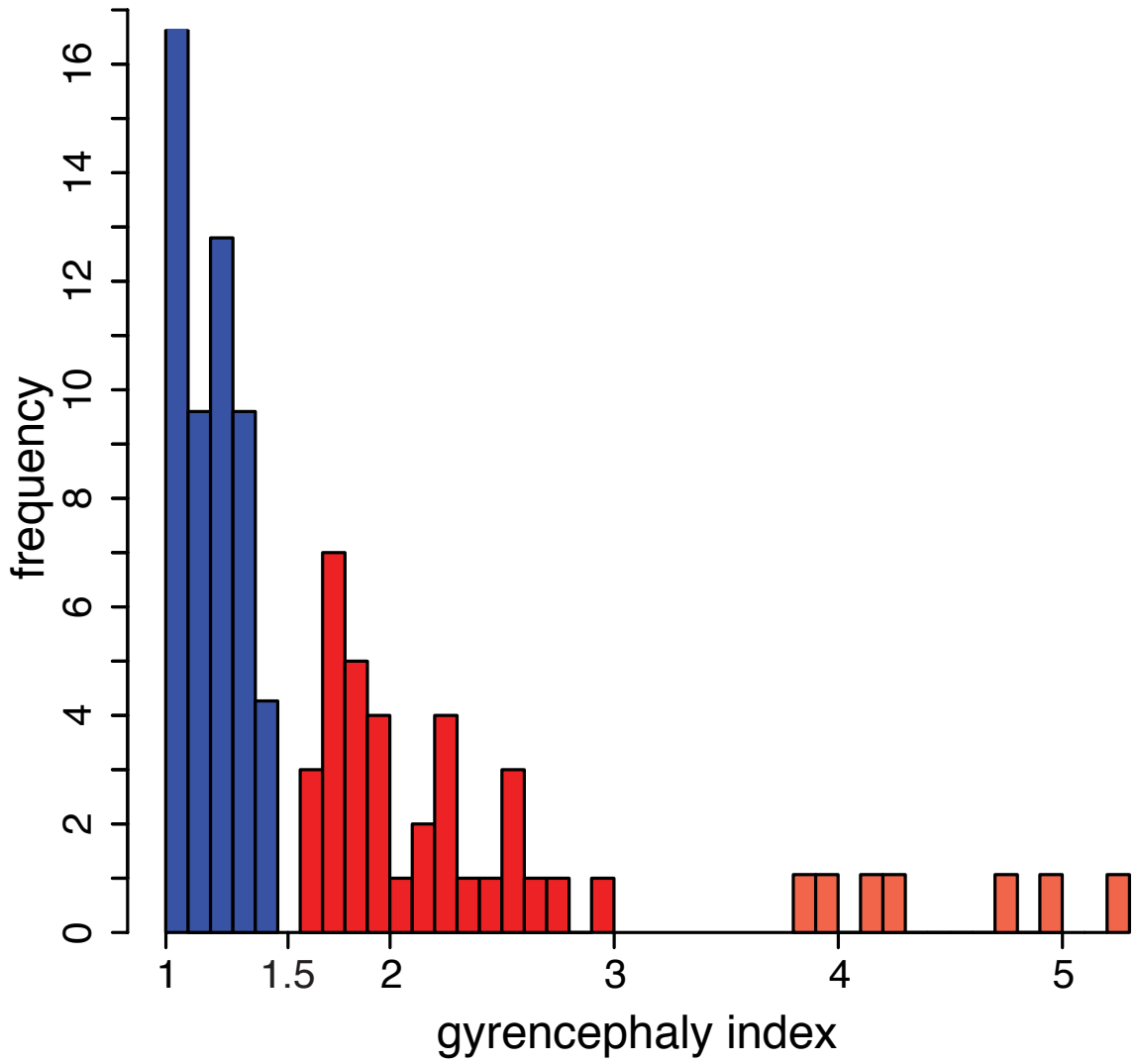

Figure S5: The bimodal distribution of GI values across the phylogeny is non-random. A histogram showing the frequency of occurrence of GI values, binned at 0.05 intervals, for the 102 mammalian species listed in Table S1. Blue, GI values $\leq$ 1.5; red, GI values $>$ 1.5. The bimodal distribution of GI values shows a natural break at GI $=$ 1.5, which is supported by energy-based hierarchical clustering (see Figure 2b). Note the possibility for a third GI group (GI $>$ 3, tomato red), constituting cetaceans and elephant; however, we have too few sampled species from these orders to assess the group decisively (see Figure S11).

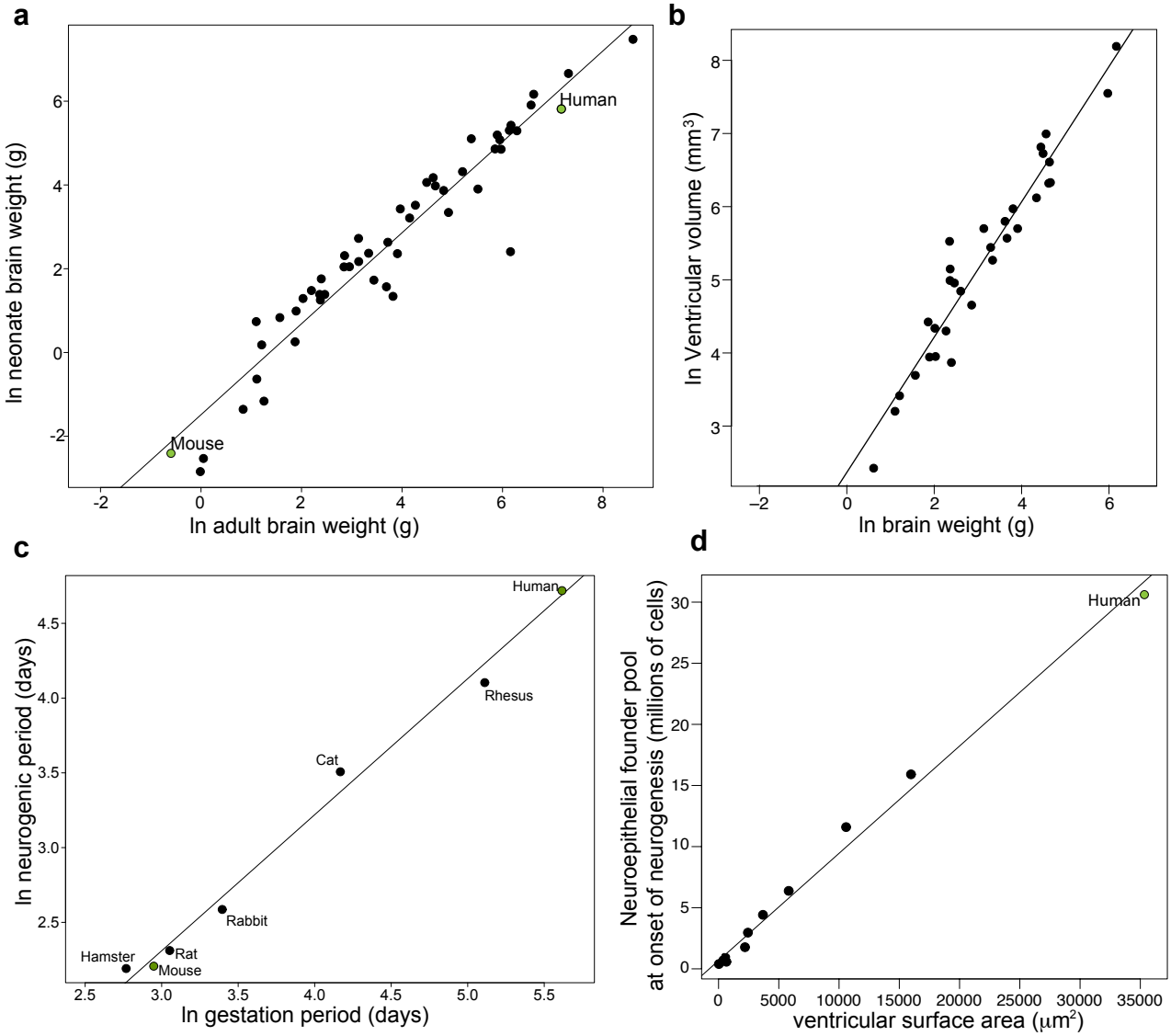

Figure S6: Ln-transformed plots of neonate brain weight (a) and ventricular volume (b) as functions of adult brain weight, neurogenic period as a function of gestation period (c); and a plot of neuroepithelial founder cells as a function of ventricular surface area (d). (a) Neonate brain weight scales linearly with adult brain weight for 52 eutherian species ($y = 1.09x - 1.49$, $R^2 = 0.92$, $P = 6 \times 10^{-7}$). (b) Ventricular volume scales linearly with adult brain weight for 30 eutherian species ($y = 0.93x + 2.37$, $R^2 = 0.93$, $P = 9 \times 10^{-8}$). (c) Neurogenic period scales linearly with gestation period for a sample of six species ($y = 0.91x - 0.42$, $R^2 = 0.94$, $P = 0.0002$), spanning two mammalian superorders. Predicted neurogenic period is shown for human. (d) Ventricular surface area, converted from ventricular volume (see Methods), scales linearly with our estimated neuroepithelial founder populations ($y = 6.7 \times 10^5 + 878x$, $R^2 = 0.94$, $P = 5 \times 10^{-8}$). (a, c) Note that these plots demonstrate the strong predictive powers of adult brain weight and gestation period for neonate brain weight and neurogenic period, respectively, validating the assumptions made in Figure 4.

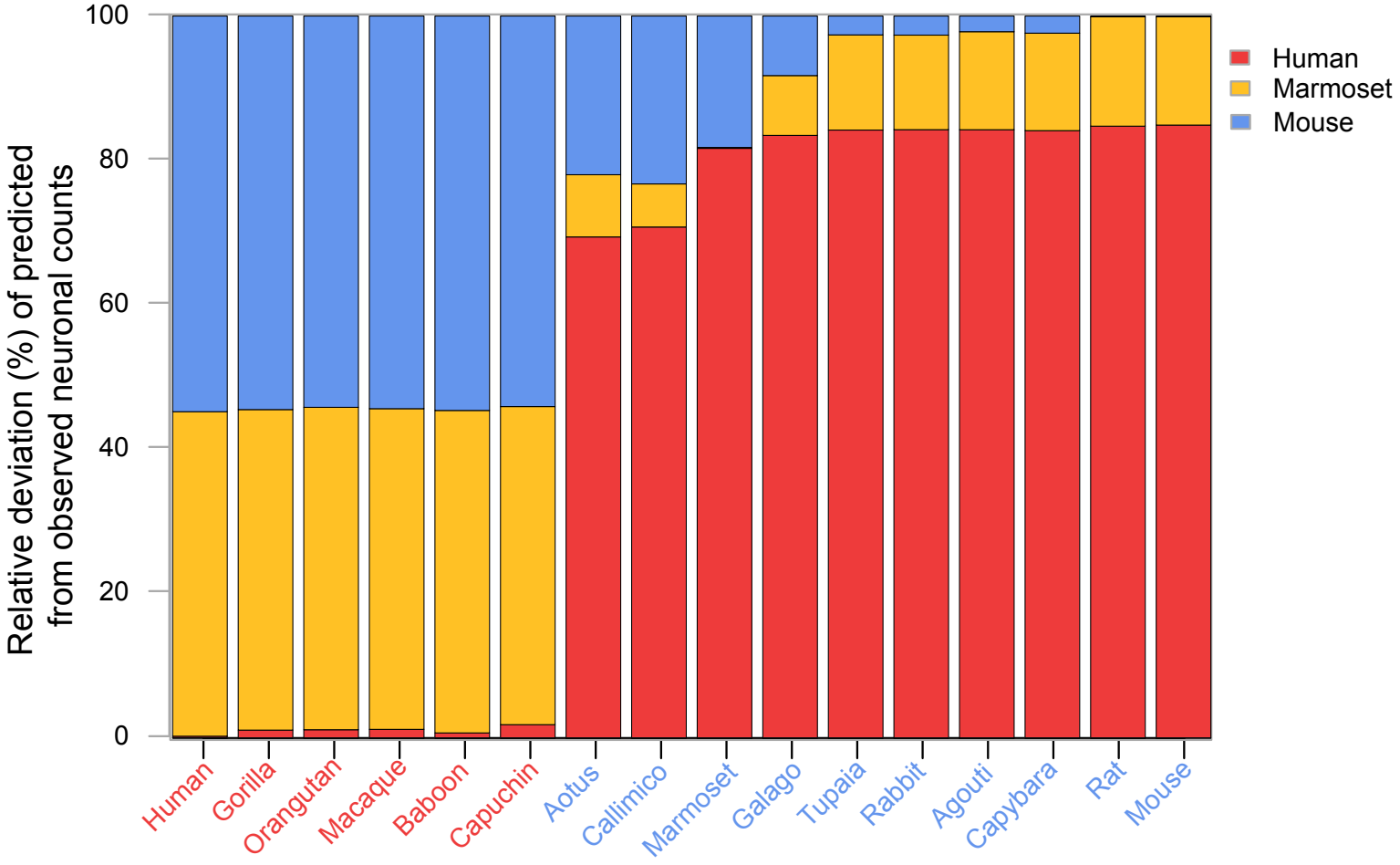

Figure S7: Stacked barplot, for the indicated species, of deviations between the observed neocortical neuron counts and the ones predicted based on human (red), mouse (blue) and marmoset (yellow) neurogenic programs (see Table 2 and Figure 5). For each species, deviations were calculated as |100*((Predicted - Observed)/Observed)| and then divided by the sum of deviations obtained for all three programs. Predictions based on the marmoset program deviate from observed neuron counts not only for the 6 species with a GI value > 1.5 (red text), but also for 8 of the 10 species with a GI ≤ 1.5 (blue text), indicating a necessity for differential proportional occurrences of bRG in low-GI species. It is worth noting that natural intraspecific variation in neocortical neuron number has been shown to be considerably less than interspecific variation (Collins et al., 2010; Young et al., 2013).

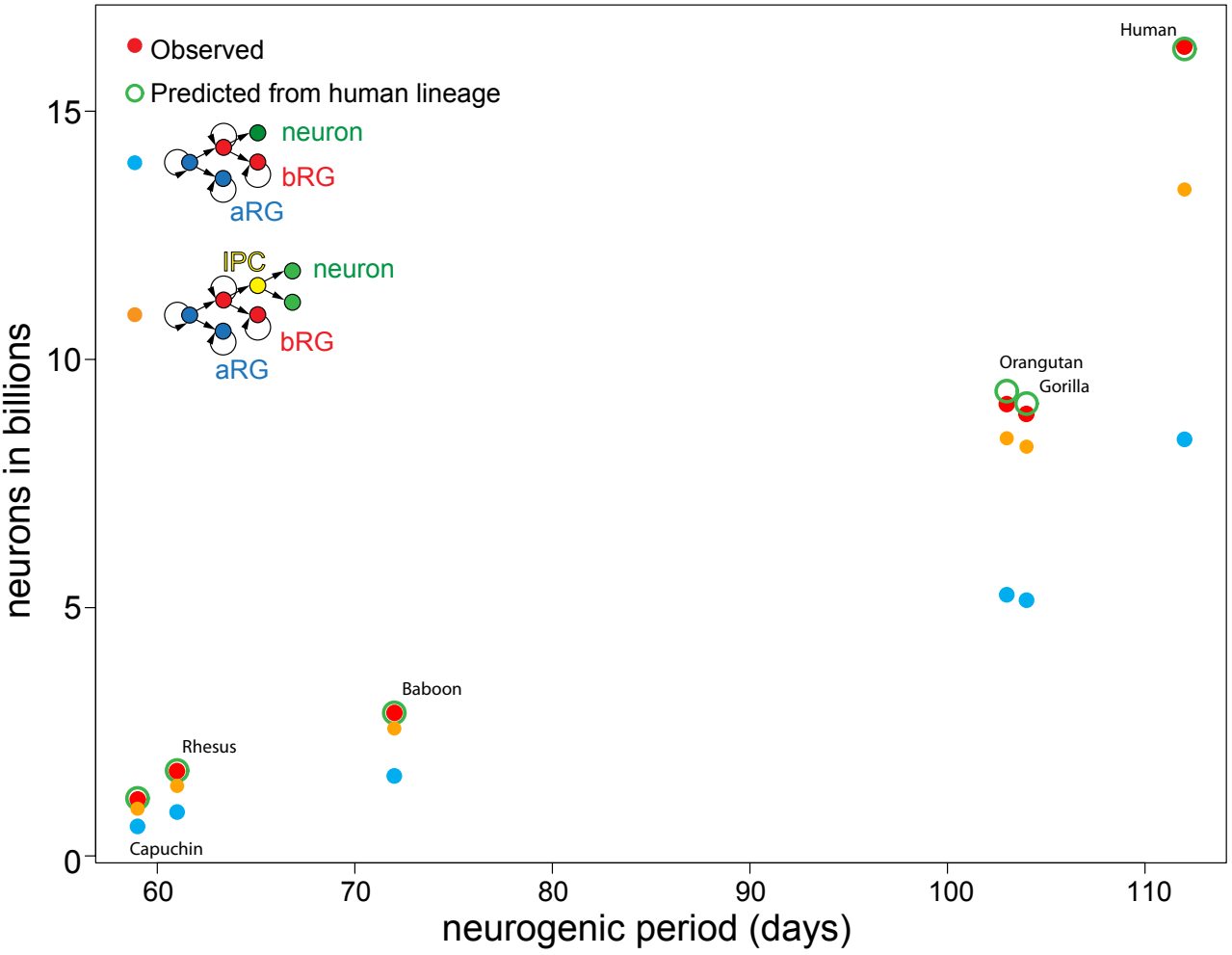

Figure S8: Plot of observed neocortical neuron number (red circles) as a function of neurogenic period for six species with a GI value > 1.5. Predicted neuron numbers are presented for the human neurogenic program (green circles; see Figure 5, Table 2) and for two further lineages, each of which is assumed to have a 100% proportional occurrence: direct neurogenesis from bRG (blue circle) and indirect neurogenesis from bRG via a self-consuming IP cell (orange circle). Note that indirect neurogenesis from bRG via IPs is nearly sufficient to achieve the observed neuronal count in the Capuchin monkey, but that 100% occurence of this lineage is unrealistic.

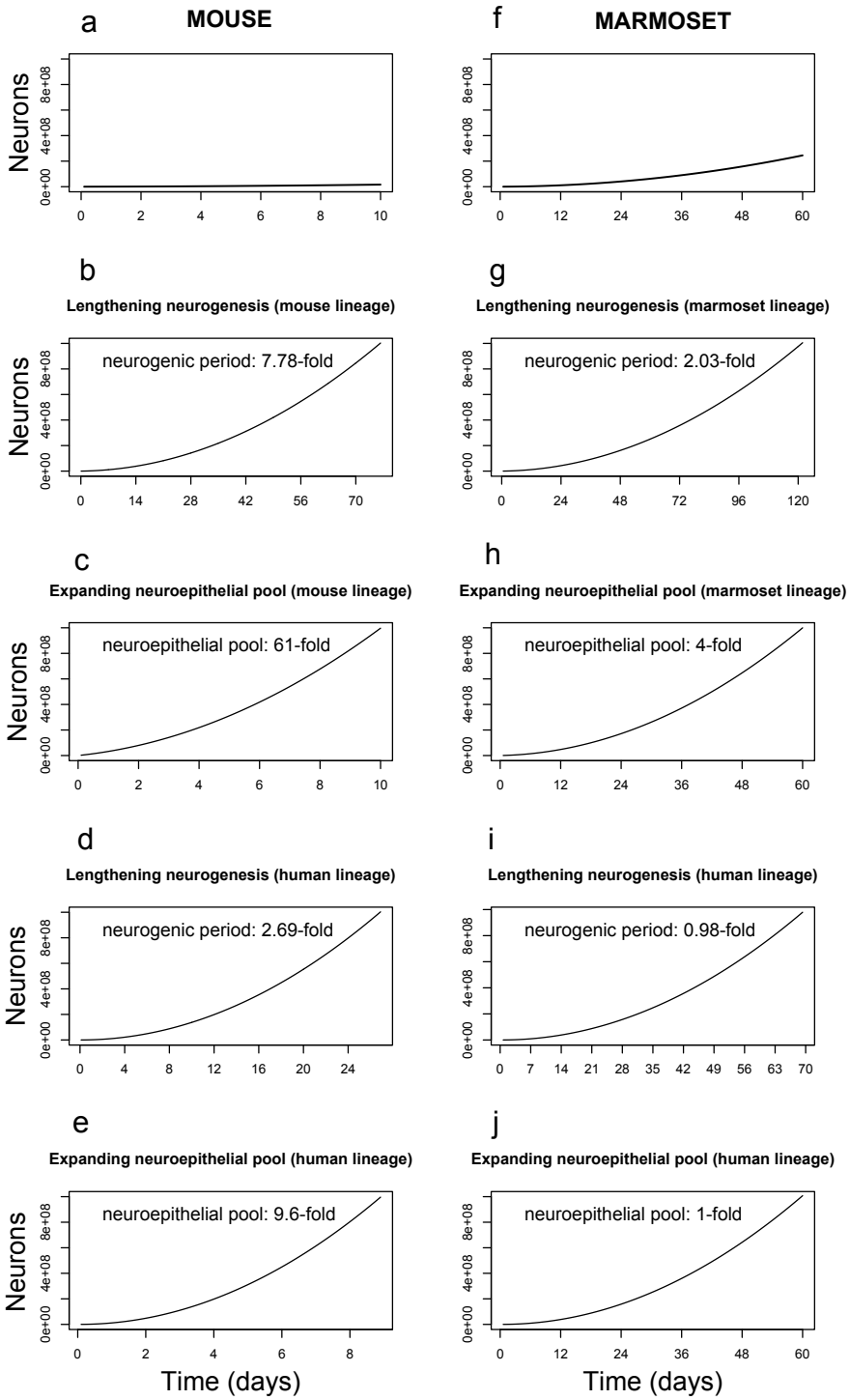

Figure S9: Calculating the adaptiveness of proliferative basal progenitors in mouse (a–e) and marmoset (f–j) in achieving 10^9 neurons with respect to lengthening neurogenic period and expanding neuroepithelial founder pool size. The fold-change of lengthening neurogenic period or expanding neuroepithelial founder pool size is indicated in each relevant plot. (a) The observed neurogenic period and founder pool size in mouse generates 1.37×10^7 neurons using the mouse neurogenic program. (b, c) Lengthening the neurogenic period (b) or expanding the founder pool size (c) using the mouse program to achieve 10^9 neurons. (d, e) Lengthening the neurogenic period (d) or expanding the founder pool size (e) using the human neurogenic program combination to achieve 10^9 neurons. (f) The observed neurogenic period and founder pool size in marmoset generates 2.45×10^8 neurons using the marmoset neurogenic program. (g, h) Lengthening the neurogenic period (g) or expanding the founder pool size (h) using the marmoset program to achieve 10^9 neurons. (i, j) Lengthening the neurogenic period (i) or expanding the founder pool size (j) using the human neurogenic program to achieve 10^9 neurons.

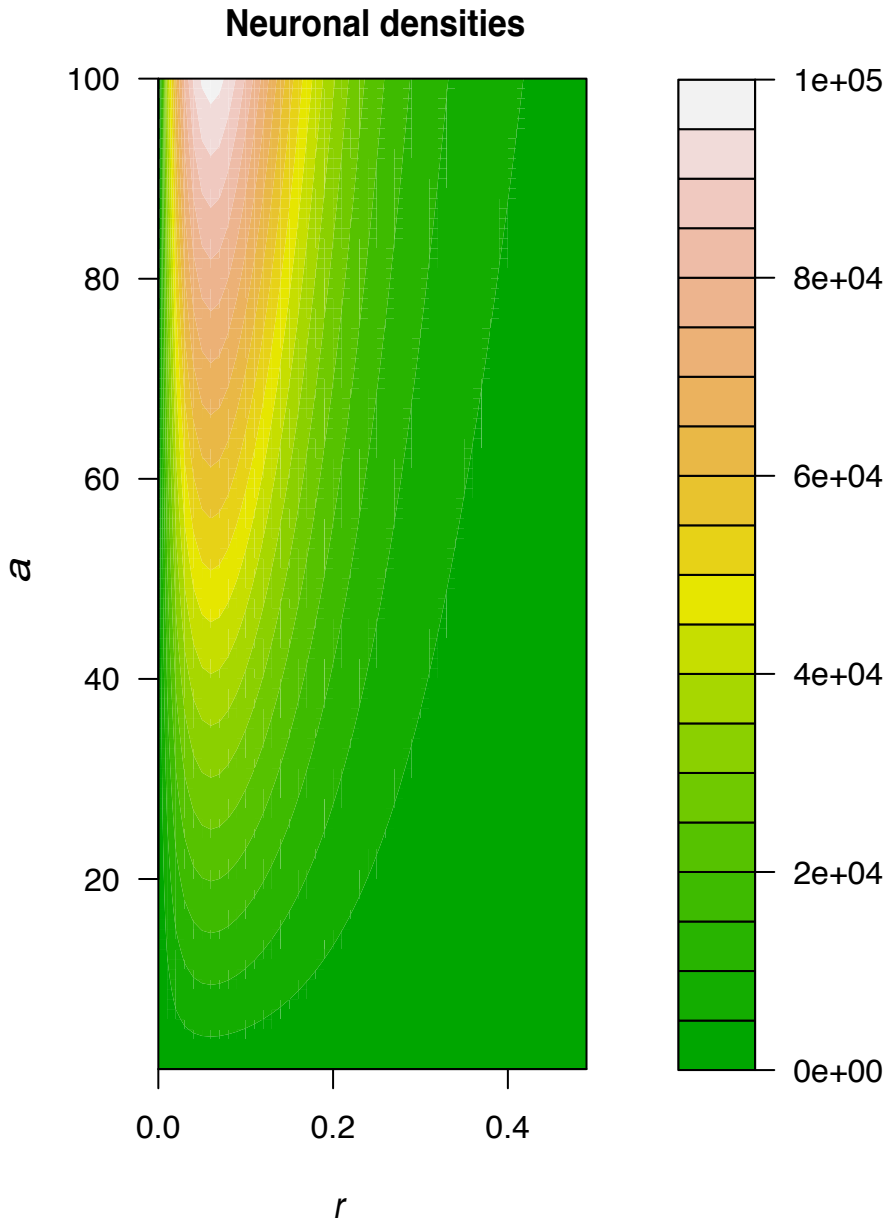

Figure S10: Neuronal outputs from solutions to ODEs describing direct *versus* indirect neurogenesis for growth-rate values ≤ 0.5. Contour plot of neuronal densities for a varying initial asymmetrically dividing cell population (a) and likelihood of direct ($r = 1$) *versus* indirect ($r = 0$) neurogenesis. Note that neuronal output increases maximally when both the initial cell pool increases ($a \to 100$) and the likelihood of indirect neurogenesis increases ($r \to 0$).

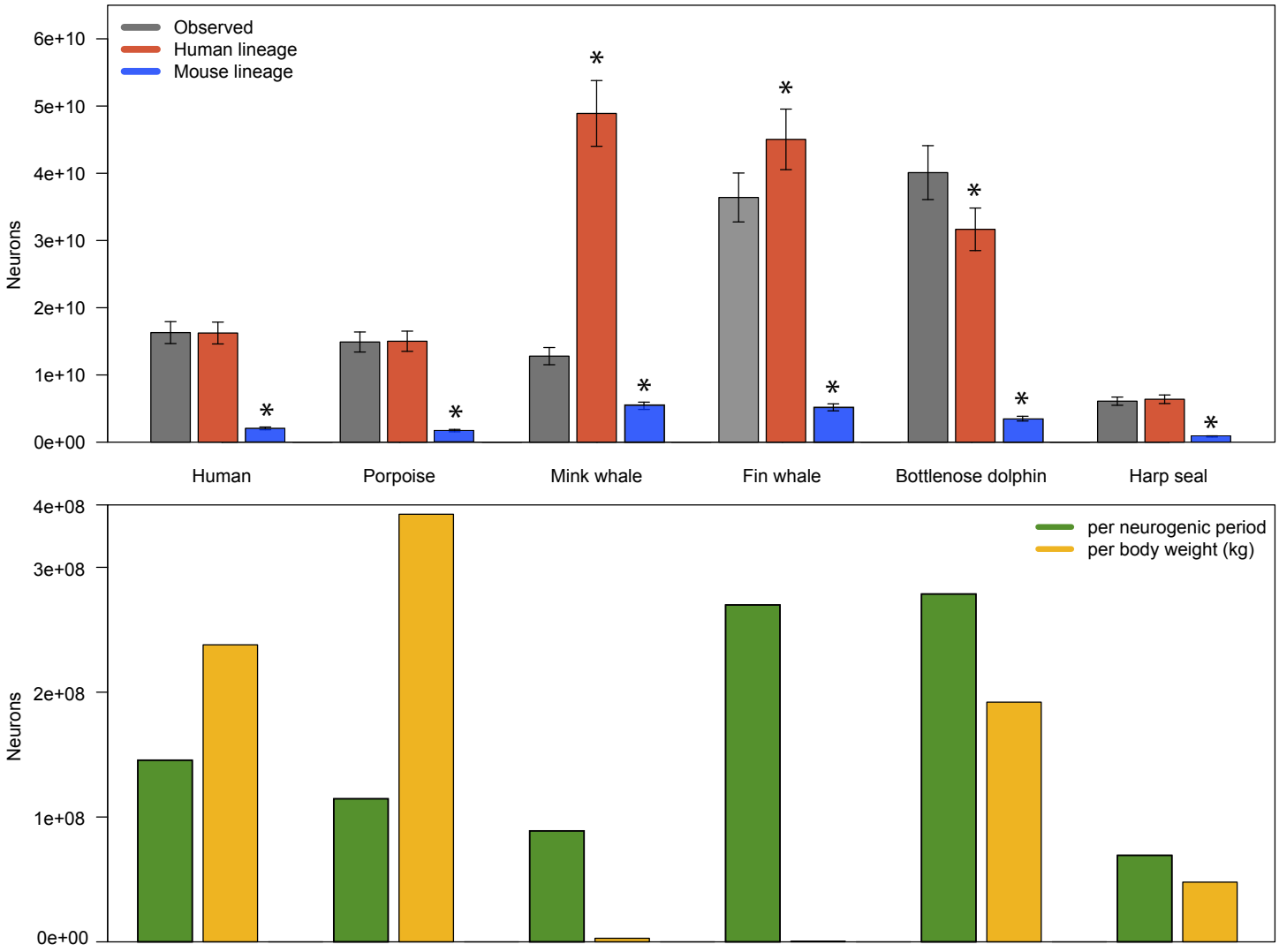

Figure S11: Neocortical development in marine mammals may be largely explained by the same neurogenic program as terrestrial mammals. (a) Observed neocortical neuron numbers for human, four cetacean species, and one marine carnivore (Harp seal) are shown beside neuron numbers calculated from the human (red) and mouse (blue) neurogenic programs (see Text). Asterisks denote neuron numbers that are significantly different ($T > 7$, $P < 0.05$) from the observed. (b) The number of neurons generated per neurogenic day (green) and per body weight (gold) in the same six species. Note that the Bottlenose dolphin is the only species for which the human program is not sufficient to achieve its observed number of neurons; and, although the fin whale generates more neurons per neurogenic day, the human program produces a higher neuron count due to the fin whale's large estimated founder pool. See Table S7 for data.

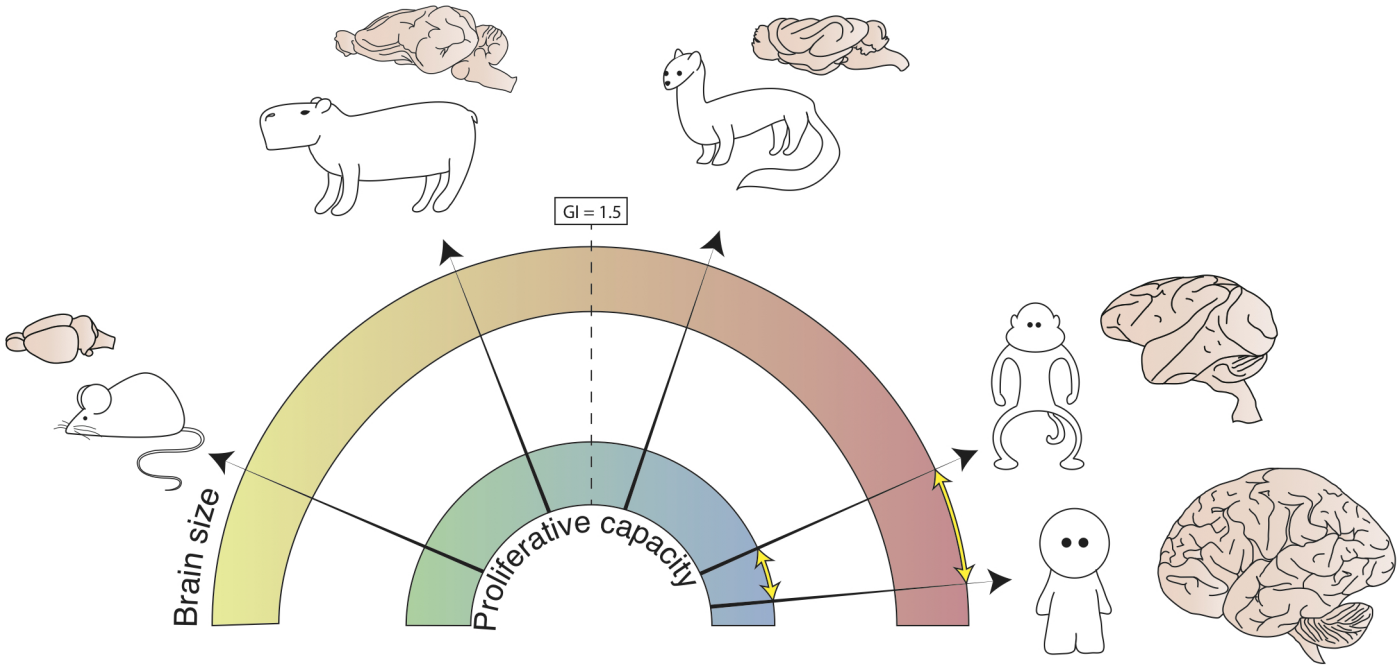

Figure S12: Neocortical complexity, represented here as cortical gyrification, is tightly linked to progenitor behavior in the OSVZ. The nature of the link, however, is such that incremental changes to OSVZ progenitor behavior (inner ring) may effect exponential changes in neocortical complexity (outer ring). Therefore, only minor changes in the proliferative capacity of basal progenitors (yellow arrow, inner ring) is needed to distinguish the major differences in neocortical complexity (yellow arrow, outer ring) between the macaque and human. It remains to be shown whether shifts in the proliferative capacity of OSVZ progenitors and neocortical complexity can occur independently (i.e., whether the arrow can be bent). Pictured clockwise: mouse, capybara, ferret, macaque, human.

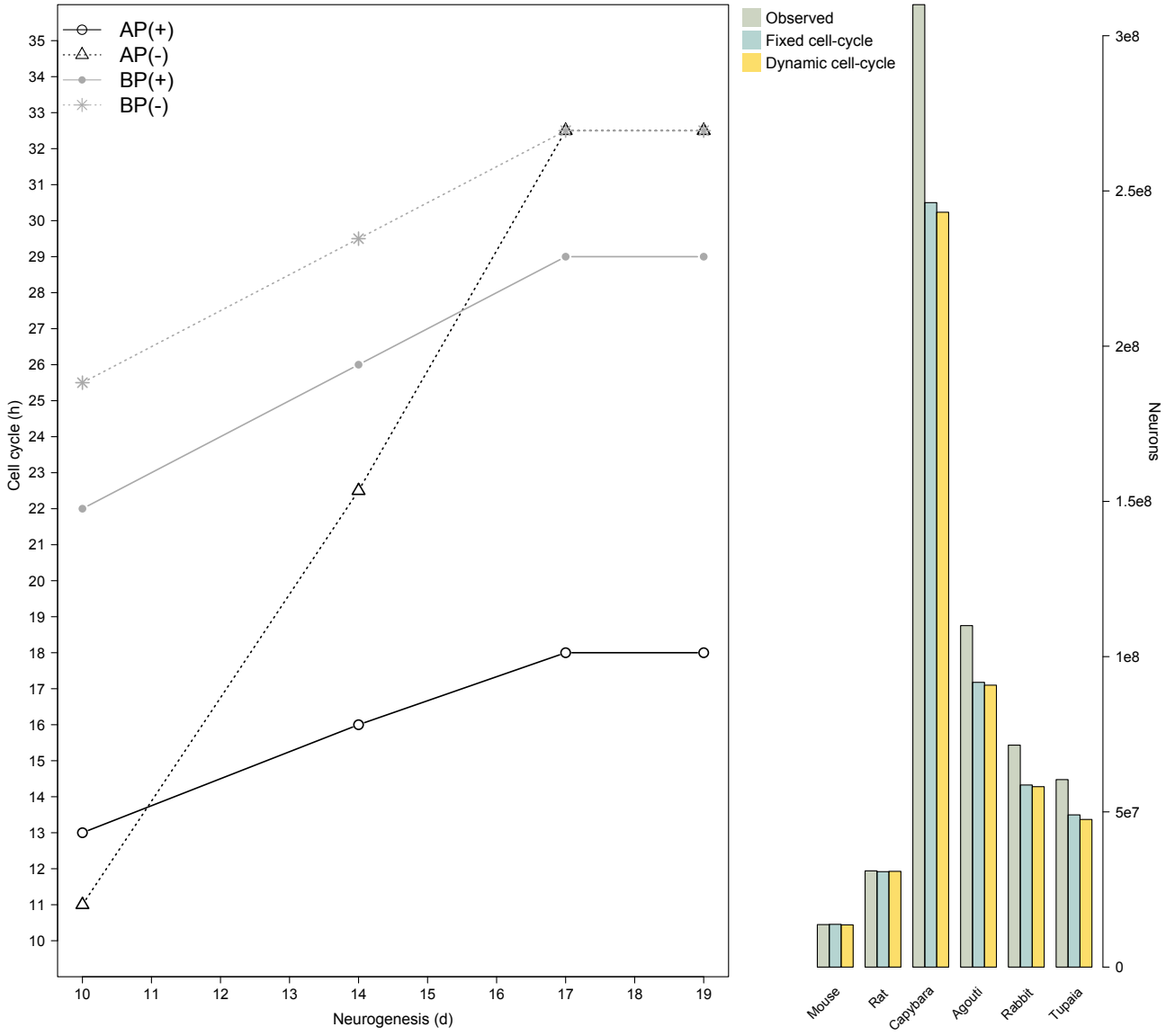

Figure S13: Cell-cycle dynamics of progenitors in non-primates. (a) Cell-cycle for $Tis21\pm$ apical and basal progenitors at different stages of neurogenesis from live-imaging studies performed in the mouse (Arai et al., 2011). (b) Barplot of the observed number of neurons in the neocortex of five rodents and a sister species to primates compared to the number of neurons predicted using a fixed cell-cycle of 18.5 hours, as was done in Figure 5, and the number of neurons predicted using dynamic cell-cycles for each progenitor as shown in (a). Note that for all species the predictions based on fixed and dynamic cell-cycles deviate by $< 1\%$. The percentage deviations between observed and mouse neurogenic program-predicted neuron numbers are listed in Table S3.

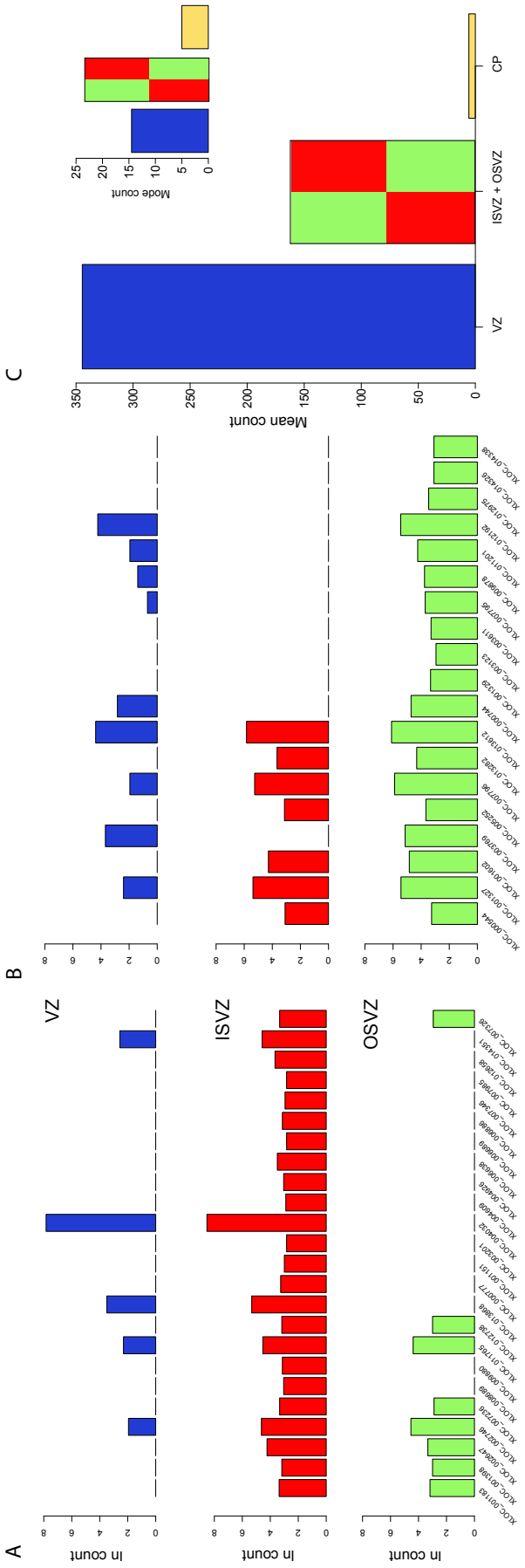

Figure S14: Germinal zone-specific transcript levels for lincRNA extracted from GW13-16 human RNA-seq. LincRNA differentially overexpressed in the (a) ISVZ and (b) OSVZ. (c) Mean and mode (inset) transcript levels for all lincRNA not differentially overexpressed in the cortical plate. See Table S8.

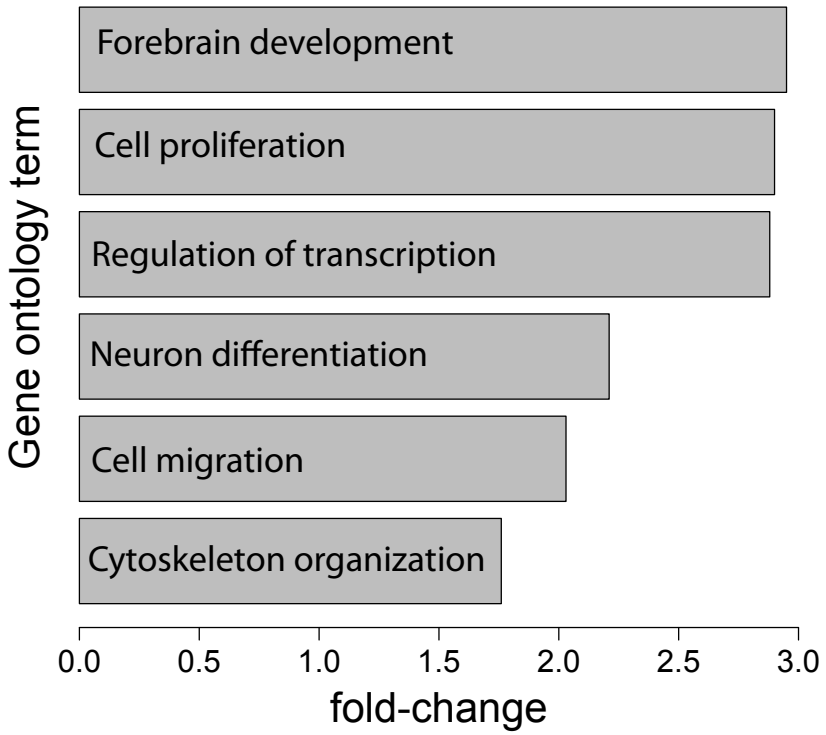

Figure S15: LincRNAs expressed during human neurogenesis tend to have gene-adjacent neighbors involved in neocortical development. Shown are fold-enrichments of Gene Ontology (GO) terms for adjacent protein-coding gene neighbors of the 142 lincRNA expressed during human neurogenesis (see Table S9). GO terms are listed if they are over-represented in the protein-coding gene set ($P < 10^{-2}$). Fold differences for enriched GO terms were analyzed using DAVID (http://david.abcc.ncifcrf.gov/summary.jsp).

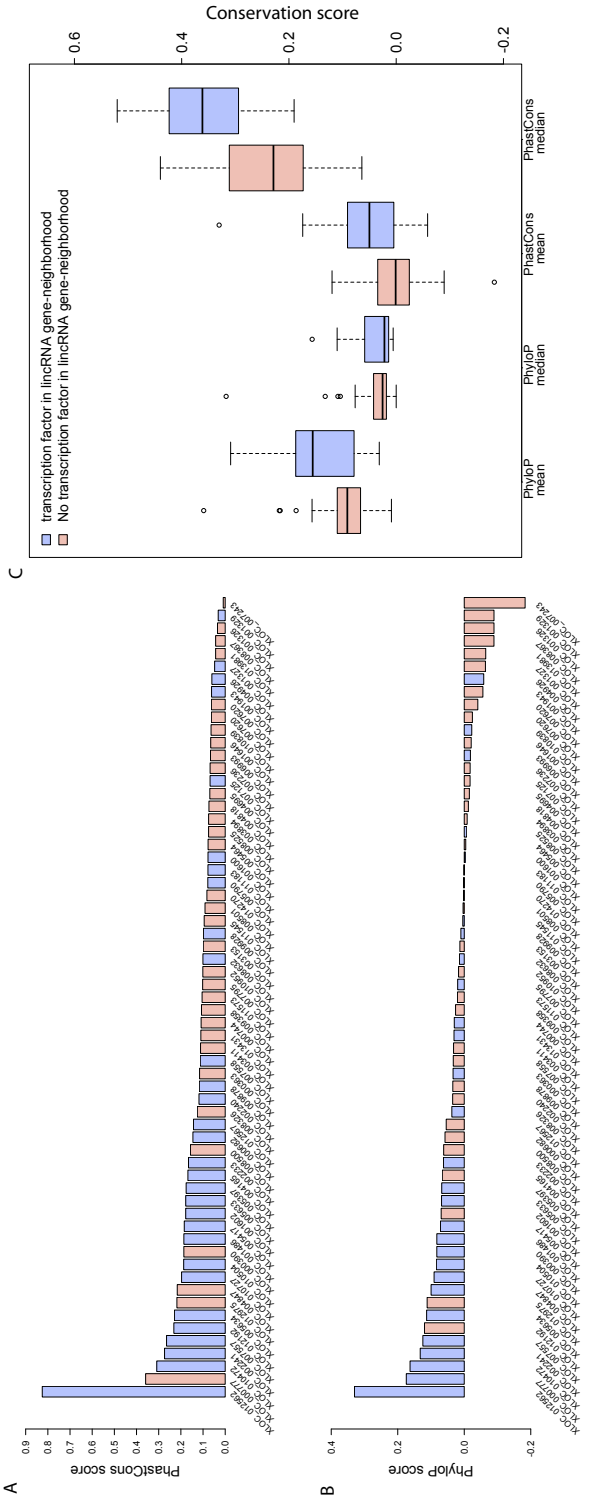

Figure S16: Sequence conservation among primates for lincRNAs expressed during human neurogenesis tends to be higher for lincRNAs flanked by at least one transcription factor. (a) The PhastCons score for 62 lincRNAs expressed during human neurogenesis, whose gene neighborhoods are not conserved in mouse. (b) PhyloP scores for the lincRNA in (a). (c) Boxplot of the mean and median PhyloP and PhastCons scores for primates for the lincRNA shown in (a,b). Mean differences for PhastCons (T = -2.371, P = .0227) and PhyloP (T = -3.513, P = 0.0009) were significantly different, but median differences were significant only for PhyloP (T = -5.211, P = 2.354e-6), not PhastCons (T = -0.706, P = 0.4847).

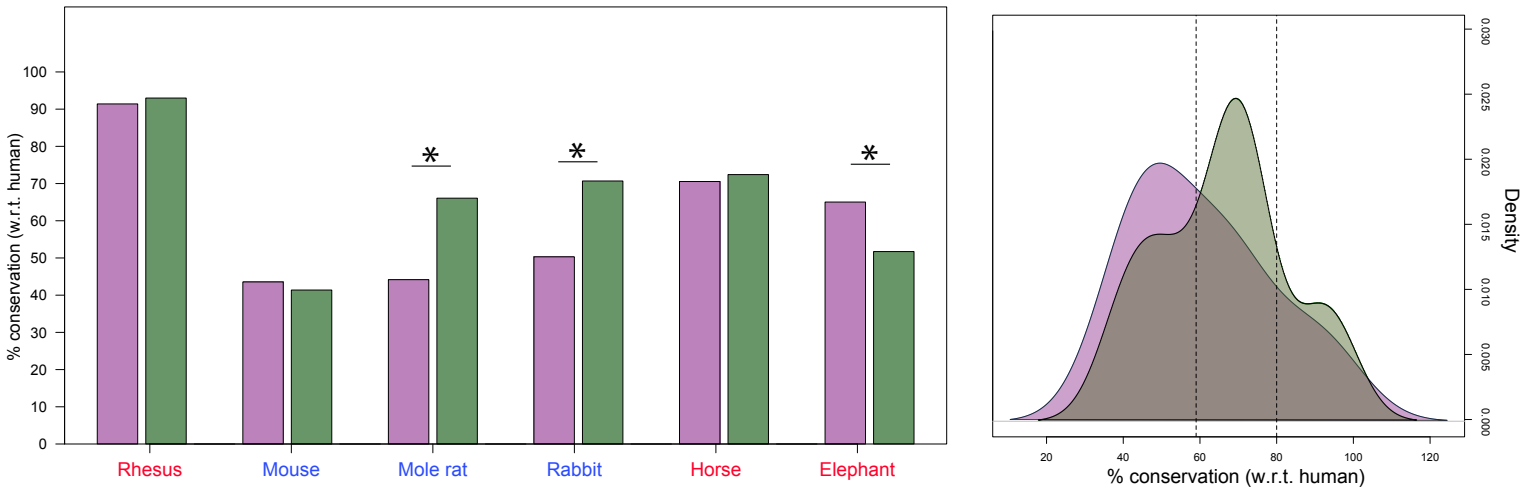

Figure S17: (a) Gene-neighborhood conservation for neurodevelopmental lincRNA (lilac) and lincRNA maximally expressed in human adipose tissue (forest green) for three high-GI (red) and three low-GI (blue) species. Conservation in the naked mole rat, rabbit, and elephant are significantly different ($P < 0.05$) for neurodevelopmental compared to adipose lincRNA, while similar levels of conservation are observed for both classes of lincRNA in rhesus monkey, mouse, and horse. (b) Density plot of conservation values in (a). The 95% confidence intervals are shown (dashed gray lines) for the peak distribution of values under a null model of evolution (i.e., an expectation model based on phylogenetic relatedness). Note that the peak distribution of adipose lincRNA, but not neurodevelopment lincRNA conservation, falls within these intervals.